A STUDY OF A LATERALLY LOADED THIN CIRCULAR CYLINDRICAL SHELL

Thesis

by

Paul H. Hayashi

In Partial Fulfillment of the Requirements

for the Degree of

Mechanical Engineer

California Institute of Technology

Pasadena, California

1957

ACKNOWLEDGMENT

The author is indebted to Professor George W. Housner at the California Institute of Technology for suggesting this problem and for his helpful guidance in solving it.

ABSTRACT

A new analysis of the stress distribution in a laterally-loaded, thin, circular, cylindrical shell is presented. It is shown that the mathematical analysis required is much simplified if the shell has zero shear strain and zero circumferential strain. With these hypotheses the stress distribution for an axial line load is calculated, and experimental measurements are made of the stresses in a shell with such a load. The computed and measured stresses agree within the limits of experimental accuracy.

It is concluded that the proposed method of stress analysis will give satisfactory values for the stresses providing the ratio of length of cylinder to radius is sufficiently large and so long as there are no abrupt variations in load intensity.

CONTENTS

I. INTRODUCTION

The established procedures for analyzing a laterally loaded thin cylindrical shell are based on the system of equilibrium differential equations given by Love.[1] The solution of these equations in even the most simple cases, results in very complicated calculations. For the solution of practical problems, writers have proposed numerous simplifications which consist essentially of dropping more or fewer smaller terms from the equations.[2] All of these analyses of thin shells are based on the thickness h of the shell being sufficiently small compared with the radius of curvature so that the stress distribution across the thickness may be taken to vary linearly. The system of equilibrium equations are linearized by restricting consideration to such cases where the stresses N_x, N_φ, $N_{x\varphi}$, (Fig. 1) are sufficiently small so that their effect on the bending is negligible. Also, the stress normal to the middle surface, σ_z , is taken to be small compared with other normal stresses and is neglected in the stress-strain relations. Since for most types of loading, the shearing stresses, $\tau_{\varphi z}$ and τ_{xz}, are small their effect is usually neglected.[2]

The simplifications introduced by previous authors lead to an eighth order partial differential equation[2,3,4] having a greater or fewer number of terms, depending upon the degree of simplification. An example is the following equation in terms of the radial displacement, ω; which is given by Naghdi and Berry.[3]

$$
\begin{aligned}
&\nabla^8 w + \frac{1}{a^4}\nabla^4 w + \frac{12(1-\nu^2)}{a^2 h}\frac{\partial^4 w}{\partial x^4} - \frac{\nu^2}{a^4}\left[\frac{\partial^4 w}{\partial x^4} - \frac{2}{(1-\nu)}\frac{\partial^4 w}{a^2\partial x^2\partial\varphi^2}\right] \\
&+ \frac{1}{a^2}\left[(2+\nu)\frac{\partial^6 w}{a^2\partial x^4\partial\varphi^2} + (3+\nu)\frac{\partial^6 w}{a^4\partial x^2\partial\varphi^4} + \frac{\partial^6 w}{a^6\partial\varphi^6}\right] + \frac{2+\nu}{a^4}\frac{\partial^4}{\partial x^2\partial\varphi^2}\nabla^2 w \\
&+ \frac{1}{a^4}\frac{\partial^4}{\partial\varphi^4}\nabla^2 w + \frac{1}{2a^6}\frac{(1+\nu)^2}{1-\nu}\frac{\partial^4 w}{\partial x^2\partial\varphi^2} - K\left[\frac{2}{1-\nu}\frac{\partial^6}{a^2\partial x^4\partial\varphi^2}\nabla^2 w + \frac{\partial^6}{a^6\partial\varphi^6}\nabla^2 w\right. \\
&\left.+ \frac{1}{a^4}\left(\frac{3-\nu}{1-\nu}\right)\frac{\partial^6}{\partial x^2\partial\varphi^4}\nabla^2 w - \frac{(1+\nu)^2}{2(1-\nu)}\frac{\partial^4}{a^2\partial x^2\partial\varphi^2}\nabla^4 w\right] + \frac{1}{aD}\left\{-\frac{\partial^3 P_x}{a^2\partial x\partial\varphi^2}\right. \qquad (1) \\
&\left.+\nu\frac{\partial^3 P_x}{\partial x^3} + (2-\nu)\frac{\partial^3 P_\varphi}{a\,\partial x^2\partial\varphi} + \frac{\partial^3 P_\varphi}{a^3\partial\varphi^3} - a\nabla^4 P_z\right\} + \frac{1}{aEh}\left\{2(1+\nu)\frac{\partial^3}{\partial x^2\partial\varphi}\nabla^2 P_\varphi\right. \\
&\left.+ (1-\nu^2)\frac{\partial^3}{a^3\partial\varphi^3}\nabla^2 P_\varphi - \frac{2(1+\nu)^3}{a^3}\frac{\partial^4 P_z}{\partial x^2\partial\varphi^2}\right\} = 0\,; \quad \nabla^4 = \text{biharmonic operator}
\end{aligned}
$$

The present study utilizes a different approach that is not based on the equations of Love and hence does not involve an equation of the type of equation (1). The solution is obtained by applying the principle of virtual displacements to the expression for the potential energy. By making the potential energy the chief consideration, it is possible to determine which factors may be neglected without introducing serious inaccuracies.

To verify the accuracy of the analysis an experimental measurement of stresses was made.

II. MIDDLE SURFACE STRAINS, SURFACE STRAINS, STRESSES, AND DEFLECTIONS OF THE SMALL CYLINDRICAL ELEMENT

The nomenclature for the stresses, strains, etc., given by Timoshenko,[2] will be used here.

Figure 1 shows an infinitesimal element of the cylindrical shell loaded by forces and moments. The location of the element is given by the distance x from the middle of the span, and the angle φ measured clockwise from the top generatrix.

The deflections of the element are shown in Fig. 1. The axial deflection u and tangential deflection v are positive when the element moves in the positive direction of x and φ respectively. The radial deflection w is positive when the element moves toward the axis of the cylinder. The shearing strain γ is positive when the shearing stress $N_{x\varphi}$ is positive. Fig. 1 shows the positive directions for all deflections and stress components.

The stress components defined here are measured per unit width of the element. The bending moments M_x, acting in the axial or longitudinal plane, and M_φ, acting in the transverse plane, are positive when they produce tension on the inner surface of the element. The twisting moment $M_{x\varphi}$ is positive when it produces tension on the inside surface along a diagonal direction of increasing values of x and φ. The stress components N_x, acting in the axial or longitudinal direction, and N_φ, acting in the transverse direction, are positive when they produce tension. The shearing stress components, $N_{x\varphi}$ and $N_{\varphi x}$, are positive when they produce tension along the diagonal of increasing values of x and φ. The radial shear stress components, Q_x and Q_φ, are positive

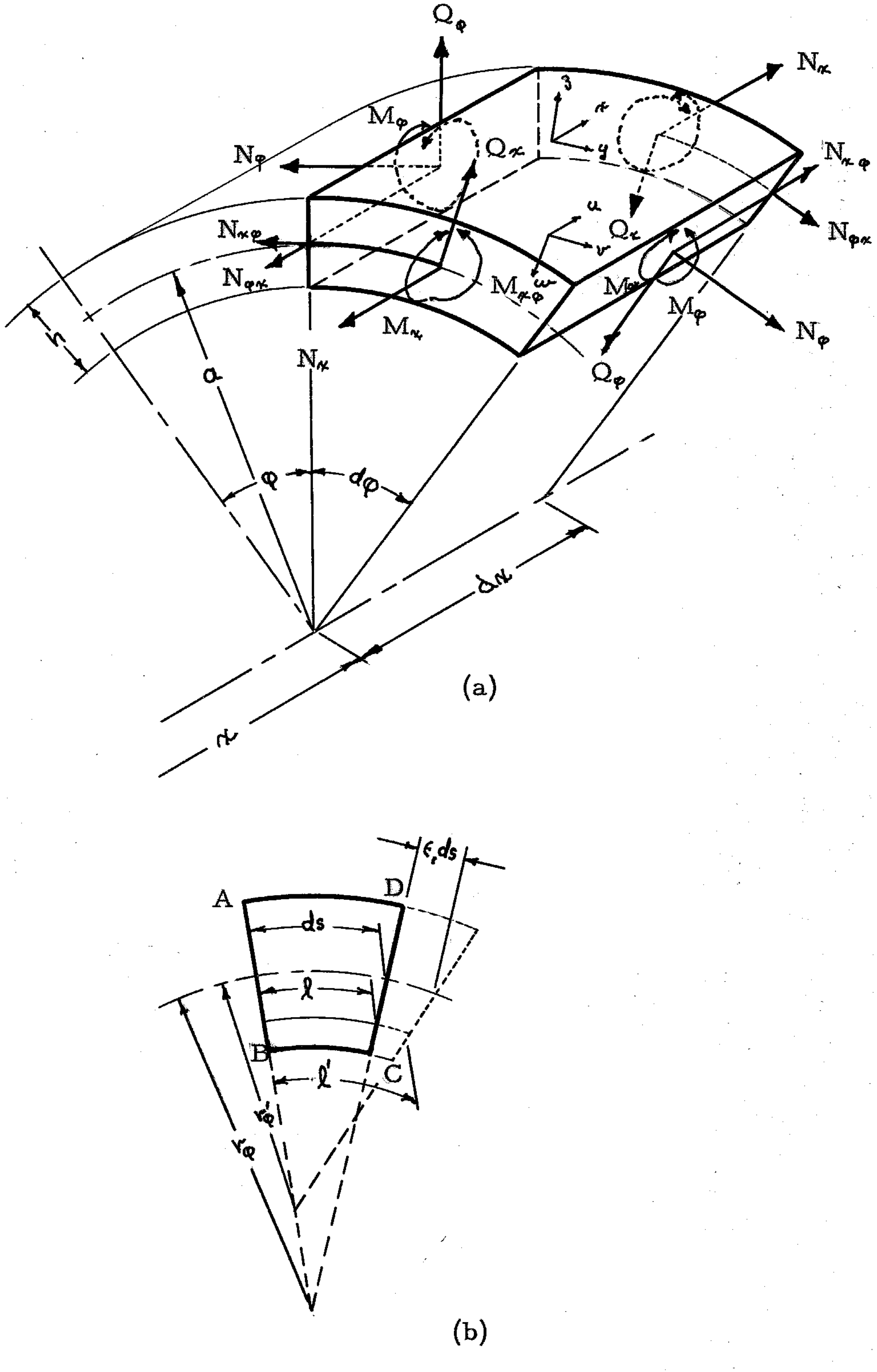

(a)

(b)

Fig. 1

when they act in an outward direction on the two sides facing nearest the origin of coordinates x and φ.

Timoshenko[2] gives the following well-known relations between middle surface strains, deflections, and stress components, applicable to the small element of length dx, width $a\,d\varphi$, constant thickness h, and radius a. The surface that bisects the thickness of the shell is called the middle surface. Thus, the transverse middle surface strain is given by:

$$\epsilon_2 = \frac{1}{a}\left(\frac{\partial v}{\partial \varphi} - w\right) = \frac{1}{Eh}\left(N_\varphi - \nu N_x\right) \tag{2}$$

The axial middle surface strain is given by:

$$\epsilon_1 = \frac{\partial u}{\partial x} = \frac{1}{Eh}\left(N_x - \nu N_\varphi\right) \tag{3}$$

The shear strain is given by:

$$\gamma = \frac{\partial v}{\partial x} + \frac{\partial u}{a\,\partial \varphi} = \frac{2 N_{x\varphi}}{Eh}(1+\nu) \tag{4}$$

The change in the longitudinal curvature is given by:

$$\chi_x = \frac{\partial^2 w}{\partial x^2} \tag{5a}$$

The change in transverse curvature by:

$$\chi_\varphi = \frac{1}{a^2}\left(w + \frac{\partial^2 w}{\partial \varphi^2}\right) = -\frac{12(1-\nu^2)}{Eh^3} M_\varphi \tag{5b}$$

The twist of the middle surface is given by:

$$\chi_{x\varphi} = \frac{1}{a}\left(\frac{\partial^2 w}{\partial \varphi\,\partial x}\right) \tag{5c}$$

The material constants, Poisson's ratio and Young's modulus, are denoted by ν and E respectively.

The surface strains, those which are directly measured at the surface, are derived from the following considerations. In the case of simple bending if r'_x and r'_φ are the values of the radii of curvature after deformation, the elongations of a thin lamina at a distance, z from the middle surface (Fig. 2) are, to a first order approximation, expressed by:

$$\epsilon_x = -z\left(\frac{1}{r_x'} - \frac{1}{r_x}\right) = -z\chi_x ; \quad \epsilon_\varphi = -z\left(\frac{1}{r_\varphi'} - \frac{1}{r_\varphi}\right) = -z\chi_\varphi \qquad (6)$$

If, in addition to bending, the sides of the element move apart, one may superpose this stretching of the middle surface on the above elongations. Let these second elongations of the middle surface be ϵ_1 and ϵ_2. One then obtains, to a first order approximation,

$$\epsilon_x = \epsilon_1 - z\chi_x \ \text{(a)} \qquad \epsilon_\varphi = \epsilon_2 - z\chi_\varphi \ \text{(b)} \qquad (7)$$

Surface strains are then obtained by substituting half the thickness of the shell, $\frac{h}{2}$, for z. Using these expressions for the components of strain of the surface lamina and assuming that there are no normal stresses between laminae ($\sigma_z = 0$), the following expressions for the components of stress are obtained:

$$\sigma_\varphi = \frac{E}{1-\nu^2}\left[\epsilon_2 + \nu\epsilon_1 - \frac{h}{2}\left(\chi_\varphi + \nu\chi_x\right)\right] \qquad (8)$$

$$\sigma_x = \frac{E}{1-\nu^2}\left[\epsilon_1 + \nu\epsilon_2 - \frac{h}{2}\left(\chi_x + \nu\chi_\varphi\right)\right] \qquad (9)$$

III; FORMULATION OF THE PROBLEM

A. Underlying Assumptions and Simplifications

Consider a thin axial strip of the circular cylindrical shell in Fig. 3. The axial stress σ in this element is produced by an elongation of the strip plus a bending of the strip, (Fig. 3b). The bending stress in the element is assumed to be given by the elementary beam theory so that it may be expressed by,

$$\sigma - \sigma_o = -E\frac{\partial^2 v}{\partial x^2}c \tag{10}$$

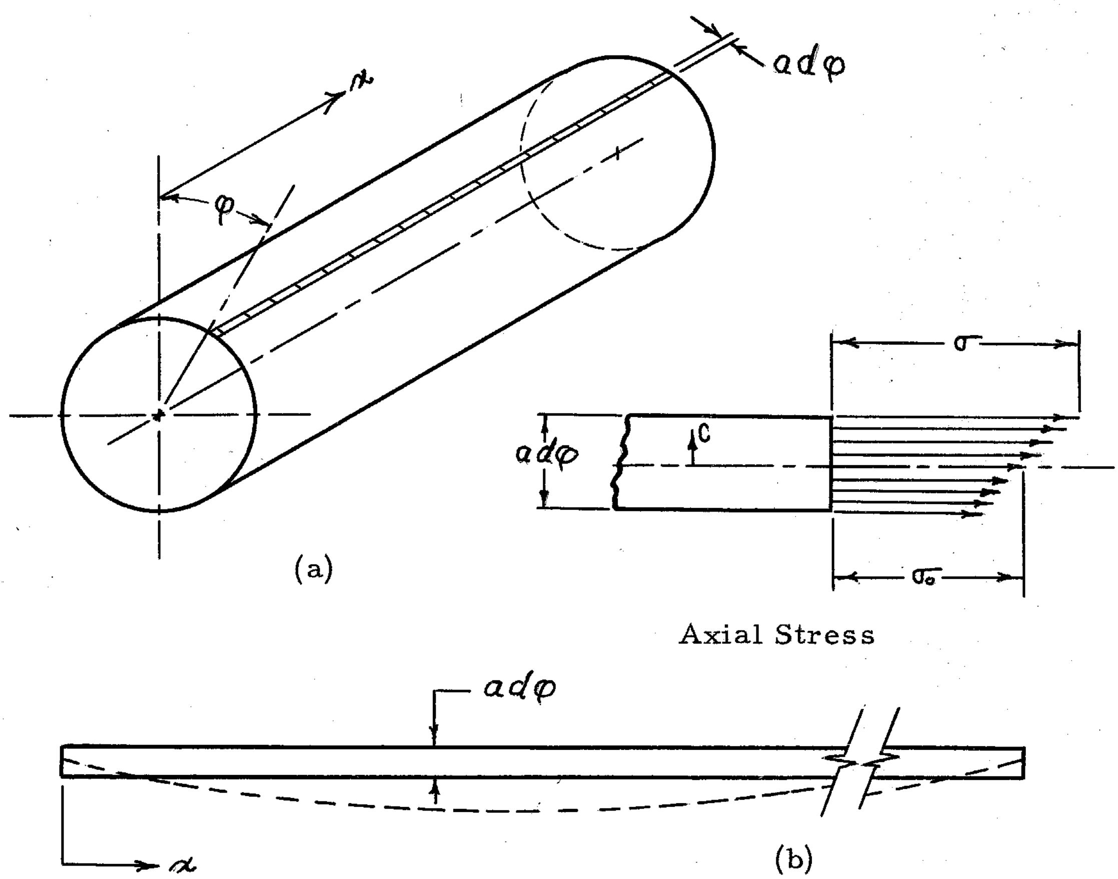

Fig. 3

Differentiating with respect to c, and noting that dc $= a\,d\varphi$, one obtains,

$$\frac{\partial \sigma}{a\partial \varphi} = -E\frac{\partial^2 v}{\partial x^2} \tag{11}$$

The elementary beam theory, (Eq. 10), requires the strain in the circumferential direction to be zero ($\epsilon_2 = 0$), so the axial stress of the element is given by,

$$\sigma = E\frac{\partial u}{\partial x} \tag{12}$$

Differentiating Eq. 12 with respect to $a\,d\varphi$ and eliminating σ by means of Eq. 11, the expression relating the axial displacement u with the tangential displacement v is obtained,

$$\frac{1}{a}\frac{\partial^2 u}{\partial x \partial \varphi} + \frac{\partial^2 v}{\partial x^2} = 0 \tag{13}$$

Integrating this expression with respect to the variable x gives,

$$\gamma_{x\varphi} = \frac{\partial u}{a\partial \varphi} + \frac{\partial v}{\partial x} = 0 \tag{14}$$

which states that the shear strain is zero. The condition $\epsilon_2 = 0$ also imposes a restriction on the displacements as follows: $\epsilon_2 = \frac{\partial v}{a\partial\varphi} - \frac{w}{a} = 0$ therefore,

$$w = \frac{\partial v}{\partial \varphi} \tag{15}$$

Equations 14 and 15 give two relations between the three components of displacement u, v, w, and if they are used, the analysis is very much simplified. Physically these relations mean that the shell is made of a material that has an infinitely large modulus of shearing rigidity as regards the shear strain $\gamma_{x\varphi}$ and an infinitely large modulus of elasticity as regards the circumferential strain ϵ_2. Although an actual shell will not have these moduli infinite the strains $\gamma_{x\varphi}$ and ϵ_2 will be small if the length of the cylinder is large compared to the radius and if the thickness is sufficiently small compared to the radius. A large class of practical applications satisfies these conditions and an analysis based on equations (14) and (15) will give the stresses and strains to a satisfactory degree of accuracy. In the vicinity of a concentrated load the strains $\gamma_{x\varphi}$ and ϵ_z may be large and in this case the computed stresses in this region may have appreciable inaccuracies.

B. Formulation of the Potential Energy

The present analysis utilizes the principle of virtual displacements so that it is necessary to formulate the expression for the strain energy of the shell. The strain energy, per unit area, of the bending moment components, M_x and M_φ is given by,[2]

$$V_{BEND.} = \frac{D}{2}\left[\chi_\varphi^2 + \chi_x^2 + 2\nu\chi_x\chi_\varphi\right] \tag{16}$$

where $D = \frac{Eh^3}{12(1-\nu^2)}$, and is called the flexural rigidity. The first term represents the energy of the transverse or cross bending. The second term represents the energy of axial plate bending. The third term is that energy produced by the simultaneous action of the two bendings.

The strain energy, per unit area, of the twisting moments $M_{x\varphi}$ and $M_{\varphi x}$ is expressed by,

$$V_{TWIST} = D(1-\nu)\,\chi_{x\varphi}^2 \tag{17}$$

The strain energy, per unit area, of the shear forces Q_x and Q_φ is given by,

$$V_{SHEAR} = \frac{1}{2}\left(\frac{Eh}{2(1+\nu)}\right)\left(\gamma_{xz}^2 + \gamma_{\varphi z}^2\right) \tag{18}$$

The strain energy, per unit area, due to stretching of the middle surface of the shell is given by,

$$V_{STRETCH.} = \frac{1}{2}\left(N_x\epsilon_x + N_\varphi\epsilon_\varphi + N_{x\varphi}\gamma_{x\varphi}\right) \tag{19}$$

The first term represents the energy of the axial extension of the middle surface. The second term represents the energy of transverse extension of the middle surface. The third term is that energy produced by the simultaneous action of the two extensions.

The total strain energy of an infinitesimal element of the cylinder is thus obtained by adding together, the energy of bending (Eq. 16), the energy of twist (Eq. 17), the energy produced by the shear forces Q_x and Q_φ(Eq. 18), and finally the energy of stretching (Eq. 19).

$$V = V_{BEND.} + V_{TWIST.} + V_{SHEAR.} + V_{STRETCH.} \qquad (20)$$

It is possible to neglect certain factors in this expression without introducing serious inaccuracies. In this analysis axial plate bending energy is small compared with the energy of cross bending and is neglected in Eq. 16. The effect of the third term in Eq. 16 has been observed to be negligible compared with the cross bending term and consequently is neglected in the present theory. The shear forces Q_x and Q_φ are small for most types of loadings, and the energy produced by these forces, (Eq. 18), is neglected in the total expression for the strain energy of the shell.

Since the conditions of negligible shear ($\gamma_{x\varphi} = 0$) and of inextension in the transverse directions ($\epsilon_\lambda = 0$) have been imposed, the stretching of the middle surface is considered to be in the axial direction only. Thus, the final two terms in Eq. 19 are omitted in the expression of the strain energy.

Integrating this expression (Eq. 20) and applying the above simplifications and Eqs 3 and 5, the strain energy for the circular cylindrical shell is obtained in terms of the displacements.

$$V = \iint \left\{ \frac{Eh}{2}\left(\frac{\partial u}{\partial x}\right)^2 + \frac{D}{2a^4}\left(w + \frac{\partial^2 w}{\partial \varphi^2}\right)^2 + \frac{D(1-\nu)}{a^2}\left(\frac{\partial^2 w}{\partial \varphi \partial x}\right)^2 \right\} a\, d\varphi\, dx \qquad (21)$$

The first two terms of the integrand are the axial beam bending extension and transverse bending energies respectively. The final term represents the energy of twisting.

C. Boundary Conditions

The tangential displacement v may be expressed in the form,

$$v = \sum_{n=1}^{\infty} f_n(x) \sin n\varphi \tag{22}$$

Applying Eqs. 14 and 15, relating the axial displacement u and radial displacement w to the tangential displacement v respectively, one obtains,

$$\begin{aligned} u &= \sum_{n=1}^{\infty} \frac{a}{n} f_n'(x) \cos n\varphi \\ w &= \sum_{n=1}^{\infty} n f_n(x) \cos n\varphi \end{aligned} \tag{23}$$

For a particular application the $f_n(x)$ must satisfy the boundary conditions at the ends. The boundary conditions depend on the nature of the restraint of the ends of the shell and on the method of support of the cylinder as a whole, i.e., built-in, free, or simply supported. Two types of restraint of the end of the shell are shown in Fig. 4.

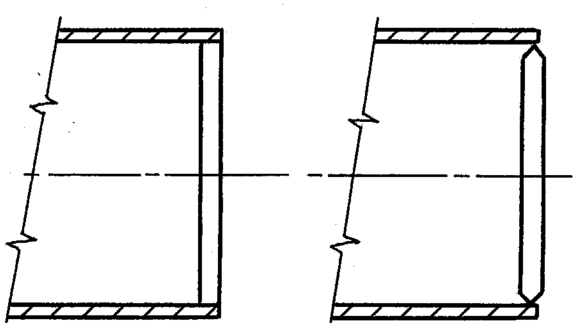

built-in (a) pin-ended (b)

Fig. 4

The particular type of shell restraint has a small effect on the stress distribution in regions away from the ends. Thus, in the case of thin shells the rim stresses are distributed only over a comparatively narrow region; this has been well established and is presented in detail by Schorer.[4] The present analysis utilizes restraint 4b.

By restricting the discussion to the case shown in Fig. 5, the analysis is much simplified. Fig. 5 shows a simply supported cylindrical shell, of circular cross-section, supported between two transverse end stiffeners (Fig. 4b), located in a plane normal to the axis of the shell. The shell is pin-ended as shown in Fig. 4b.

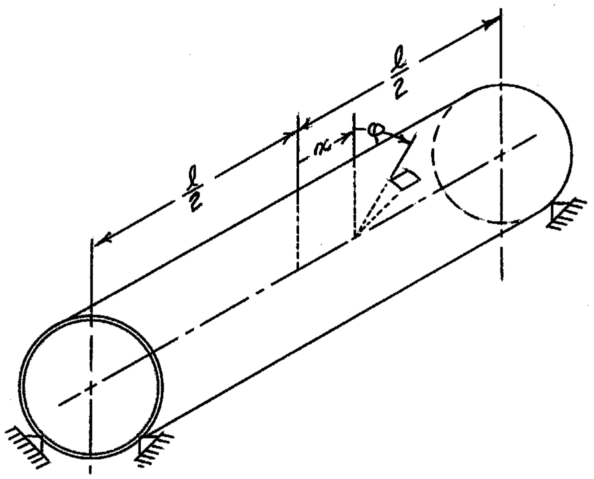

Fig. 5

This represents a typical and practical application since tubes or circular shells, subject to continuous surface loads require circumferential stiffening members at the supports, as in the case of pipe lines, tanks, etc.

The boundary conditions at the two ends, located in the coordinate system shown in Fig. 5, are: At $x = \pm \frac{l}{2}$

$$\begin{aligned} w &= 0 \\ \frac{\partial^2 w}{\partial x^2} &= 0 \\ v &= 0 \\ \frac{\partial u}{\partial x} &= 0 \end{aligned} \tag{24}$$

Choosing the eigen functions appropriate to these boundary conditions, the displacements may be expressed by,

$$v = \sum_{m,n}^{\infty} A_{m,n} \sin n\varphi \cos \frac{m\pi}{\lambda} x \tag{25a}$$

$$u = -\sum_{m,n}^{\infty} a A_{m,n}\left(\frac{m\pi}{\ell}\right)\frac{1}{n}\cos n\varphi \sin\frac{m\pi}{\ell}x \tag{25b}$$

$$w = \sum_{m,n}^{\infty} A_{m,n}(n) \cos n\varphi \cos\frac{m\pi}{\ell}x \tag{25c}$$

It should be noted that for $n = 1$, the displacements are:

$$v = \sum_{m}^{\infty} A_m \sin\varphi \cos\frac{m\pi}{\ell}x \tag{26a}$$

$$u = -\sum_{m}^{\infty} a A_m \left(\frac{m\pi}{\ell}\right) \cos\varphi \sin\frac{m\pi}{\ell}x \tag{26b}$$

$$w = \sum_{m}^{\infty} A_m \cos\varphi \cos\frac{m\pi}{\ell}x \tag{26c}$$

This represents a purely vertical displacement without distortion of the cross-section. Thus, the radial deflection of the shell at the top generatrix, ($\varphi = 0$), due to the contribution of the first transverse harmonic ($n = 1$) is the expression obtained by the elementary beam theory where deformation of the cross section is not considered.[5] Therefore, the contributions to the displacements from the higher transverse harmonics ($n > 1$) are "corrections" applied to the simple beam theory.

D. The Radial Concentrated Load Problem

In the immediate vicinity of a concentrated force the strains $\gamma_{x\varphi}$ and ϵ_x will have an appreciable effect. However, over the remainder of the shell, the simplified expression for the strain energy (Eq. 21) will describe the state of stress with satisfactory accuracy.

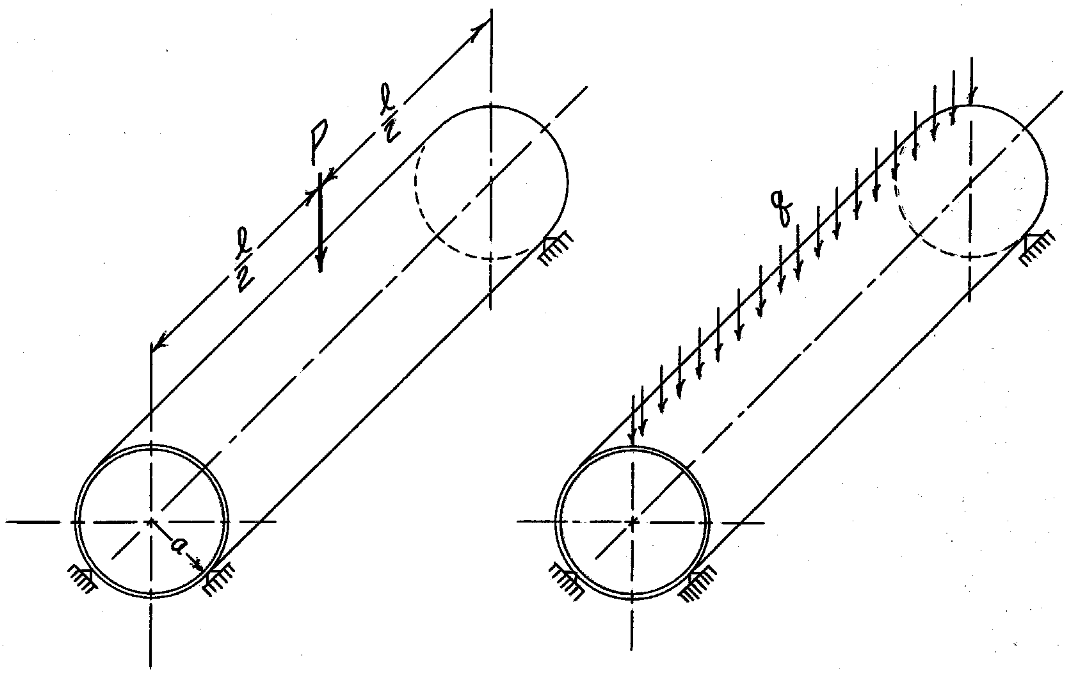

(a) (b)

Fig. 6

Fig. 6a shows a radially directed, concentrated force applied on the top generatrix mid-way between the two transverse end stiffeners, ($x = 0, \varphi = 0$). The shell is simply supported at each end.

To obtain the coefficient, $A_{m,n}$ in the expression for the displacements, the principle of virtual displacements is employed.

$$\delta W = \delta V \tag{27}$$

The work done by the force P, as a result of an infinitely small variation in the radial displacement, is

$$\delta W = P\delta w = \left\{ P\delta A_{m'n'} \, n' \cos n'\varphi \cos \frac{m'\pi x}{l} \right\}_{x=0,\, \varphi=0} = P\delta A_{m'n'} \, n' \tag{28}$$

Equating this to the variation of potential energy and solving for the coefficient, $A_{m,n}$ there is obtained:

$$A_{m,n} = \frac{2P}{\pi^5 Eh}\left(\frac{l}{a}\right)^3 \frac{1}{m^4 n\left[\frac{1}{n^4} + \frac{(1-n^2)^2}{\pi^4 m^4 (1-\nu^2)12}\left(\frac{l}{a}\right)^4\left(\frac{h}{a}\right)^2 + \left(\frac{n}{m}\right)^2 \frac{h^2 l^2}{(6)(1+\nu)\pi^2 a^4}\right]} \qquad (29)$$

E. <u>The Uniform Radial Line Load Problem</u>

Fig. 6b shows a uniform radial line load extending the full length of the top generatrix, $(\varphi=0)$. The line load of intensity q lbs per in., produces a virtual work, as a result of an infinitely small variation in the radial displacements, that is given by:

$$\delta W = \left\{ q\,\delta A_{m'n'}\, n' \cos n'\varphi \int_{-\frac{l}{2}}^{+\frac{l}{2}} \cos\frac{m'\pi}{l}x\,dx \right\}_{\varphi=0} = q\,\delta A_{m'n'}\, n' \frac{2l}{m'\pi}\sin\frac{m'\pi}{2} \qquad (30)$$

Equating this to δV there is obtained:

$$A_{m,n} = \frac{2q}{\pi^5 Eh}\left(\frac{l}{a}\right)^3\left(\frac{2l}{\pi}\right) \frac{\sin\frac{m\pi}{2}}{m^5 n\left[\frac{1}{n^4} + \frac{(1-n^2)^2}{\pi^4 m^4 (1-\nu^2)(12)}\left(\frac{l}{a}\right)^4\left(\frac{h}{a}\right)^2 + \left(\frac{n}{m}\right)^2 \frac{h^2 l^2}{6(1+\nu)\pi^2 a^4}\right]} \qquad (31)$$

Eqs. 29 and 31, therefore, in conjunction with Eq. 25 express the displacements, u, v, and w, for the concentrated load and the line load respectively.

Differentiating the axial displacement u with respect to the axial coördinate x, the expression for the unit axial middle surface strain is obtained.

$$\epsilon_1 = \frac{\partial u}{\partial x} = -\sum_{m,n}^{\infty} A_{m,n}\left(\frac{a}{n}\right)\left(\frac{m\pi}{l}\right)^2 \cos n\varphi \cos\frac{m\pi}{l}x \qquad (32)$$

Applying Eq. 5b, similarly, for the change in transverse curvature, one obtains,

$$\chi_\varphi = \frac{1}{a^2}\left(w + \frac{\partial^2 w}{\partial \varphi^2}\right) = \sum_{m,n}^{\infty} A_{m,n}\frac{(1-n^2)}{a^2} n \cos n\varphi \cos\frac{m\pi}{l}x \qquad (33)$$

IV. APPLICATION OF THE THEORY TO A SPECIFIC CIRCULAR CYLINDER

To verify the analysis with measured results a cylinder was made with the following dimensions:

ℓ = 45.0 inches, length

a = 3.367 inches, constant cross sectional radius

h = 0.015 inches, shell thickness

The shell material was steel with Young's modulus and Poisson's ratio of 30 x 10^6 psi and 0.3 respectively.

For simplicity in the calculations, the following notation is adopted:

$$K \equiv \frac{2}{\pi^5 E h}\left(\frac{\ell}{a}\right)^3$$

$$L \equiv \left(\frac{\ell}{a}\right)^4 \left(\frac{h}{a}\right)^2 \frac{1}{\pi^4 (1-\nu^2)(12)} \tag{34}$$

$$Q \equiv \frac{h^2 \ell^2}{6(1+\nu)\pi^2 a^4}$$

With this notation and the application of Eqs. 31, 29, and 25, the following expressions for the displacements are obtained. For the radial concentrated load problem the displacements are expressed by,

$$\frac{v}{P} = K \sum_{m,n}^{\infty} \frac{\sin n\varphi \cos \frac{m\pi}{\ell} x}{m^4 n \left[\frac{1}{n^4} + L\left(\frac{1-n^2}{m^2}\right)^2 + Q\left(\frac{n}{m}\right)^2\right]} \tag{35a}$$

$$\frac{u}{P} = -K\pi\left(\frac{a}{\ell}\right) \sum_{m,n}^{\infty} \frac{\cos n\varphi \sin \frac{m\pi}{\ell} x}{m^3 n^2 \left[\frac{1}{n^4} + L\left(\frac{1-n^2}{m^2}\right)^2 + Q\left(\frac{n}{m}\right)^2\right]} \tag{35b}$$

$$\frac{w}{P} = K \sum_{m,n}^{\infty} \frac{\cos n\varphi \cos \frac{m\pi}{\ell} x}{m^4 \left[\frac{1}{n^4} + L\left(\frac{1-n^2}{m^2}\right)^2 + Q\left(\frac{n}{m}\right)^2\right]} \tag{35c}$$

For the uniform line load problem the displacements are expressed by,

$$\frac{v}{q} = 2K\left(\frac{\ell}{\pi}\right)\sum_{m,n}^{\infty} \frac{\sin n\varphi \cos\frac{m\pi}{\ell}x \sin\frac{m\pi}{2}}{m^5 n\left[\frac{1}{n^4} + L\left(\frac{1-n^2}{m^2}\right)^2 + Q\left(\frac{n}{m}\right)^2\right]} \tag{36a}$$

$$\frac{u}{q} = -2Ka\sum_{m,n}^{\infty} \frac{\cos n\varphi \sin\frac{m\pi}{\ell}x \sin\frac{m\pi}{2}}{m^4 n^2\left[\frac{1}{n^4} + L\left(\frac{1-n^2}{m^2}\right)^2 + Q\left(\frac{n}{m}\right)^2\right]} \tag{36b}$$

$$\frac{w}{q} = 2K\left(\frac{\ell}{\pi}\right)\sum_{m,n}^{\infty} \frac{\cos n\varphi \cos\frac{m\pi}{\ell}x \sin\frac{m\pi}{2}}{m^5\left[\frac{1}{n^4} + L\left(\frac{1-n^2}{m^2}\right)^2 + Q\left(\frac{n}{m}\right)^2\right]} \tag{36c}$$

The constants appearing in these series and defined by Eq. 34, when evaluated for this cylinder, are:

$$K = 34.64 \times 10^{-6} \; [\text{in/lb}]$$
$$L = 595.328 \times 10^{-6} \; [0]$$
$$Q = 46.05 \times 10^{-6} \; [0]$$

A typical example of the calculations is presented below. The radial deflections, w, of the shell at the mid-span are calculated for a uniform radial line load extending along the top generatrix (Fig. 6b). These radial deflections are given by Eq. 33c. When the axial distance, x, is set equal to zero, the resulting expression (Eq. 37) is a double Fourier series with transverse harmonics indicated by mode number, n, and axial harmonics indicated by mode number, m. The series has been evaluated through the eighth ($n = 8$) transverse mode and seventh ($m = 7$) axial mode.

Results of sufficient accuracy for most practical applications would be obtained with fewer terms. For example, evaluating the series through the seventh axial harmonic and through the following number of transverse harmonics gives results for the radial displacement with these accuracies: $n = 4$, 7 percent; $n = 5$, 3 percent; $n = 6$, 1 percent.

RADIAL DEFLECTION AT THE MID-SPAN TRANSVERSE CROSS SECTION FOR THE UNIFORM RADIAL LINE LOAD

$$\frac{10^6}{993.353}\,\frac{w}{q} = \sum_{m,n}^{\infty} \frac{\cos n\varphi \,\sin\frac{m\pi}{2}}{m^5\left[\frac{10^6}{n^4} + 595.33\left(\frac{1-n^2}{m^2}\right)^2 + 46.05\left(\frac{n}{m}\right)^2\right]} \tag{37}$$

TABLE 1. Transverse Harmonic Contributions to Radial Displacement

A. First harmonic, $n = 1$.

$$\frac{10^6}{993.353}\,\frac{w}{q} = \cos\varphi \sum_{m}^{\infty} \frac{\sin\frac{m\pi}{2}}{m^5}$$

m	m^5	$(m^5)^{-1}$
1	1	1.0000
3	243	0.0041
5	3,125	0.0003
7	16,807	0.0001
		0.996

B. Second harmonic, $n = 2$

$$\frac{1}{993.353}\,\frac{w}{q} = \cos 2\varphi \sum_{m}^{\infty} \frac{\sin\frac{m\pi}{2}}{62506.12\,m^5 + 5357.95\,m + 103.72\,m^3}$$

m	m^3	m^5	$62{,}506.12m^5$	$5{,}357.95m$	$103.72m^3$	(Σ)	$\Sigma^{-1} \times 10^6$
1	1	1	62,506.12	5,357.75	103.72	+67,968	+14.713
3	27	243	15,188,987.16	16,073.85	2,800.44	−15,207,861	− .066
5	125	3,125	195,331,625.00	26,789.75	12,965.00	+195,371,380	+ .005
7	343	16,807	1,050,540,358.84	37,505.65	35,575.46	−1,050,613,441	− .001
9	729	59,049	3,690,923,879.88	48,221.55	75,611.88	+3,691,047,714	+ .0003
11	1,331	161,051	10,066,673,132.12	58,937.45	138,051.32	−10,066,870,121	− .0001
							14.651

C. Third harmonic, $n = 3$

$$\frac{1}{993.353}\,\frac{w}{q} = \cos 3\varphi \sum_{m}^{\infty} \frac{\sin\frac{m\pi}{2}}{12352\,m^5 + 328\,m^3 + 38101\,m}$$

m	m^3	m^5	$12{,}352m^5$	$328m^3$	$38{,}101m$	(Σ)	$(\Sigma)^{-1} \times 10^6$
1	1	1	12,352	328	38,101	50,801	+19.685
3	27	243	3,001,536	8,856	114,303	3,124,695	− .320
5	125	3,125	38,600,000	41,000	190,505	38,831,505	+ .026
7	343	16,807	207,600,064	112,504	266,707	207,979,275	− .005
9	729	59,049	729,373,248	239,112	342.909	729,955,269	+ .0014
11	1,331	161,051	1,989,301,952	436,568	419,111	1,990,157,631	− .0005
13	2,197	371,293	4,586,211,136	720,616	495,313	4,587,427,065	+ .0002
15	3,375	759,375	9,379,800,000	1,107,000	571,515	9,381,478,515	− .0001
							19.387

D. Fourth harmonic, $n = 4$

$$\frac{1}{993.353}\,\frac{w}{q} = \cos 4\varphi \sum_{m}^{\infty} \frac{\sin \frac{m\pi}{2}}{3912\, m^5 + 648\, m^3 + 133{,}949\, m}$$

m	m^3	m^5	$3{,}912m^5$	$648m^3$	$133{,}949m$	(Σ)	$(\Sigma)^{-1} \times 10^6$
1	1	1	3,912	648	133,949	138,509	+ 7.220
3	27	243	950,616	17,496	401,847	1,369,959	− .730
5	125	3,125	12,225,000	81,000	669,745	12,975,745	+ .077
7	343	16,807	65,748,984	222,264	937,643	66,908,891	− .015
9	729	59,049	230,999,688	472,392	1,205,541	232,677,621	+ .004
11	1,331	161,051	630,031,512	862,488	1,473,439	632,367,439	− .0016
13	2,197	371,293	1,452,498,216	1,423,656	1,741,337	1,455,663,209	+ .0007
15	3,375	759,375	2,970,675,000	2,187,000	2,009,235	2,974,871,235	− .0003
17	4,913	1,419,857	5,554,480,584	3,183,624	2,277,133	5,559,941,341	+ .0002
19	6,859	2,476,099	9,686,499,288	4,444,632	2,545,031	9,693,488,951	− .0001
							6.555

E. Fifth harmonic, $n = 5$

$$\frac{1}{993.353}\,\frac{w}{q} = \cos 5\varphi \sum_{m}^{\infty} \frac{\sin \frac{m\pi}{2}}{1606\, m^5 + 1062\, m^3 + 342909\, m}$$

m	m^3	m^5	$1{,}606m^5$	$1{,}062m^3$	$342{,}909m$	(Σ)	$(\Sigma)^{-1} \times 10^6$
1	1	1	1,606	1,062	342,909	345,577	+ 2.894
3	27	243	390,258	28,674	1,028,727	1,447,659	− .691
5	125	3,125	5,018,750	132,750	1,714,545	6,866,045	+ .146
7	343	16,807	26,992,042	364,266	2,400,363	29,756,671	− .034
9	729	59,049	94,832,694	774,198	3,086,181	98,693,073	+ .010
11	1,331	161,051	258,647,906	1,413,533	3,771,999	263,833,427	− .004
13	2,197	371,293	596,296,558	2,333,214	4,457,817	603,087,589	+ .0016
15	3,375	759,375	1,219,556,250	3,584,250	5,143,635	1,228,284,135	− .0008
17	4,913	1,419,857	2,280,290,342	5,217,606	5,829,453	2,291,227,401	+ .0005
19	6,859	2,476,099	3,976,614,994	7,284,258	6,515,271	3,990,414,523	− .0003
21	9,261	4,084,101	6,559,066,206	9,835,182	7,201,089	6,576,102,477	+ .0002
23	12,167	6,436,343	10,336,766,858	12,921,354	7,886,907	10,357,575,119	− .0001
							2.322

F. Sixth harmonic, $n = 6$

$$\frac{1}{993.353}\,\frac{w}{q} = \cos 6\varphi \sum_{m}^{\infty} \frac{\sin \frac{m\pi}{2}}{778\, m^5 + 1567\, m^3 + 729{,}277\, m}$$

m	m^3	m^5	$778m^5$	$1{,}567m^3$	$729{,}277m$	(Σ)	$(\Sigma)^{-1} \times 10^6$
1	1	1	778	1,567	729,277	731,622	+1.367
3	27	243	189,054	42,309	2,187,831	2,419,194	− .413
5	125	3,125	2,431,250	195,875	3,646,385	8,692,704	+ .115
7	343	16,807	13,075,846	537,481	5,104,939	18,718,266	− .053
9	729	59,049	45,940,122	1,142,343	6,563,493	53,645,958	+ .019
11	1,331	161,051	125,297,678	2,085,677	8,022,047	135,405,402	− .007
13	2,197	371,293	288,865,954	3,442,699	9,480,601	301,789,254	+ .003
15	3,375	759,375	590,793,750	55,288,625	10,939,155	607,021,530	− .0016
17	4,913	1,419,857	1,104,648,746	7,698,671	12,397,709	1,124,745,117	+ .0009
19	6,859	2,476,099	1,926,405,022	10,748,053	13,856,263	1,951,009,338	− .0005
21	9,261	4,084,101	3,177,430,578	14,511,987	15,314,817	3,191,943,565	+ .0003
23	12,167	6,436,343	5,007,476,410	19,065,689	16,773,371	5,043,315,470	− .0002
25	15,625	9,765,625	7,597,656,250	24,484,375	18,231,925	7,640,372,550	+ .0001
							1.030

G. Seventh harmonic, $n = 7$

$$\frac{1}{993.353}\,\frac{w}{q} = \cos 7\varphi \sum_{m}^{\infty} \frac{\sin\frac{m\pi}{2}}{423\,m^5 + 2167\,m^3 + 1{,}371{,}636\,m}$$

m	m^3	m^5	$423m^5$	$2{,}167m^3$	$1{,}371{,}636m$	(Σ)	$(\Sigma)^{-1} \times 10^6$
1	1	1	423	2,167	1,371,636	1,374,226	+0.728
3	27	243	102,789	58,509	4,114,908	4,276,206	− .234
5	125	3,125	1,321,875	270,875	6,858,180	8,450,930	+ .118
7	343	16,807	7,109,361	743,281	9,601,452	17,454,094	− .057
9	729	59,049	24,977,727	1,579,743	12,344,724	38,902,194	+ .026
11	1,331	161,051	68,124,573	2,884,277	15,087,996	86,096,846	− .012
13	2,197	371,293	157,056,939	4,760,899	17,831,268	179,649,106	+ .0056
15	3,375	759,375	321,215,625	7,313,625	20,574,540	349,103,790	− .0029
17	4,913	1,419,857	600,599,511	10,646,471	23,317,812	634,563,794	+ .0016
19	6,859	2,476,099	1,047,389,877	14,863,453	26,061,084	1,088,314,414	− .0009
21	9,261	4,084,101	1,727,574,723	20,068,587	28,804,356	1,776,447,666	+ .0006
23	12,167	6,436,343	2,722,572,089	26,365,889	31,547,628	2,780,486,000	− .0004
25	15,625	9,765,625	4,130,859,375	33,859,375	34,290,900	4,199,009,650	+ .0001
							0.580

H. Eighth harmonic, $n = 8$

$$\frac{1}{993.333}\,\frac{w}{q} = \cos 8\varphi \sum_{m}^{\infty} \frac{\sin\frac{m\pi}{2}}{250\,m^5 + 2858\,m^3 + 2{,}362{,}857\,m}$$

m	m^3	m^5	$250m^5$	$2{,}858m^3$	$2{,}362{,}857m$	(Σ)	$(\Sigma)^{-1} \times 10^6$
1	1	1	250	2,858	2,362,857	2,365,965	+0.423
3	27	243	60,750	77,166	7,088,571	7,226,487	− .138
5	125	3,125	781,250	357,250	11,814,285	12,952,785	+ .077
7	343	16,807	4,201,750	980,294	16,539,999	21,722,043	− .046
9	729	59,049	14,762,250	2,083,482	21,265,713	38,111,445	+ .026
11	1,331	161,051	40,262,750	3,803,998	25,991,427	70,058,175	− .014
13	2,197	371,293	92,823,250	6,279,026	30,717,141	129,819,417	+ .008
15	3,375	759,375	189,843,750	9,645,750	35,442,855	364,751,772	− .003
17	4,913	1,419,857	354,964,250	14,041,354	40,168,569	409,174,173	+ .002
19	6,859	2,476,099	619,024,750	19,603,022	44,894,283	683,522,055	− .0015
21	9,261	4,084,101	1,021,025,250	26,467,938	49,619,997	1,097,113,185	+ .0009
23	12,167	6,436,343	1,609,085,750	34,773,286	54,345,711	1,698,204,747	− .0006
25	15,625	9,765,625	2,441,406,250	44,656,250	59,071,425	2,545,133,925	+ .0004
27	19,683	14,348,907	3,587,226,750	56,254,014	63,797,139	3,707,277,903	− .0003
29	24,389	20,511,149	5,127,787,250	69,703,762	68,522,853	5,266,013,865	+ .0002
31	29,791	28,629,151	7,157,287,750	85,142,678	73,248,587	7,315,678,995	− .0001
33	35,937	39,135,393	9,783,848,250	102,707,946	77,974,281	9,964,530,477	+ .0001
							0.334

TABLE 2. SUMMATION OF THE TRANSVERSE HARMONIC CONTRIBUTIONS TO THE RADIAL DISPLACEMENT

ϕ	$0.996 \cos\phi$	$14,651 \cos 2\phi$	$19.387 \cos 3\phi$	$6.555 \cos 4\phi$	$2.322 \cos 5\phi$	$1.030 \cos 6\phi$	$0.580 \cos 7\phi$	$0.334 \cos 8\phi$	$\frac{10^6}{993.353} \frac{w}{q}$
0	0.996	14.651	19.387	6.555	2.322	1.030	0.580	0.334	45.855
10	.981	13.768	16.789	5.021	1.493	0.515	.198	.058	38.823
20	.936	11,223	9.694	–1.141	–0.404	– .515	– .444	– .314	21.317
30	.863	7.325	0	–3.277	–2.011	–1.030	– .502	– .167	1.201
45	.704	0	–13.707	–6.555	–1.642	0	.410	.334	–20.456
60	.498	– 7.325	–19.387	–3.277	1.161	1.030	.290	– .167	–27.177
70	.341	–11.223	–16.789	1.141	2.287	.515	– .373	– .314	–24.415
90	0	–14.651	0	6.555	0	–1.030	0	.334	– 8.792
105	– .258	–12.688	13.707	3.277	–2.243	0	.560	– .167	2.188
125	– .572	– 5.011	18.726	–5.021	–0.203	.892	– .526	.058	8.343
150	– .863	7.325	0	–3.277	2.011	–1.030	.502	– .167	4.501
165	– .962	12.688	–13.707	3.277	– .601	0	.151	– .167	1.881
180	– .996	14.651	–19.387	6.555	–2.322	1.030	– .580	.334	– 0.715

Figure 7 shows the radial deflection as a function of the coordinate φ (Eq. 37c), at the mid-span cross section under the applied uniform radial line load (Table II). Figure 8 is a curve showing similar results (see Appendix) obtained for the case of the single radial concentrated load as in Fig. 5a.

From Eqs. 32 and 31 for the uniform radial line load, the following expression for the direct unit axial strain is obtained:

$$\epsilon_1 = \frac{\partial u}{\partial x} = -K(2) q\, \pi \left(\frac{a}{\ell}\right) \sum_{n,m}^{\infty} \frac{\cos n\varphi \cos \frac{m\pi}{\ell} x \sin \frac{m\pi}{2}}{m^3 n^2 \left[\frac{1}{n^4} + L\left(\frac{1-n^2}{m^2}\right)^2 + Q\left(\frac{n}{m}\right)^2\right]} \tag{38}$$

Figure 9 shows the unit axial strain ϵ_1, of the middle surface at the mid-span transverse cross section as a function of "beam depth" y. The numerical calculations appear in the Appendix.

Using Eq. 33 for the change in transverse curvature, Eq. 31 for the coefficient $A_{m,n}$ for the line load, and the notation of Eq. 34, the change in transverse curvature is expressed by,

$$\chi_\varphi = \frac{1}{a^2}\left(w + \frac{\partial^2 w}{\partial \varphi^2}\right) = Kq\left(\frac{2\ell}{\pi}\right)\frac{1}{a^2} \sum_{m,n}^{\infty} \frac{(1-n^2)\cos n\varphi \cos \frac{m\pi}{\ell} x \sin \frac{m\pi}{2}}{m^5 \left[\frac{1}{n^4} + L\left(\frac{1-n^2}{m^2}\right)^2 + Q\left(\frac{n}{m}\right)^2\right]} \tag{39}$$

Figure 10 shows the change in transverse curvature at the mid-span cross section as a function of the coordinate, φ . The series expression, Eq. 39, is identical with Eq. 36c for the radial deflection w, except for the coefficient $\frac{1-n^2}{a^2}$ in each term. Thus, the bulk of the numerical calculation has been performed in the foregoing sample calculation. The calculations for this curve are presented in the Appendix.

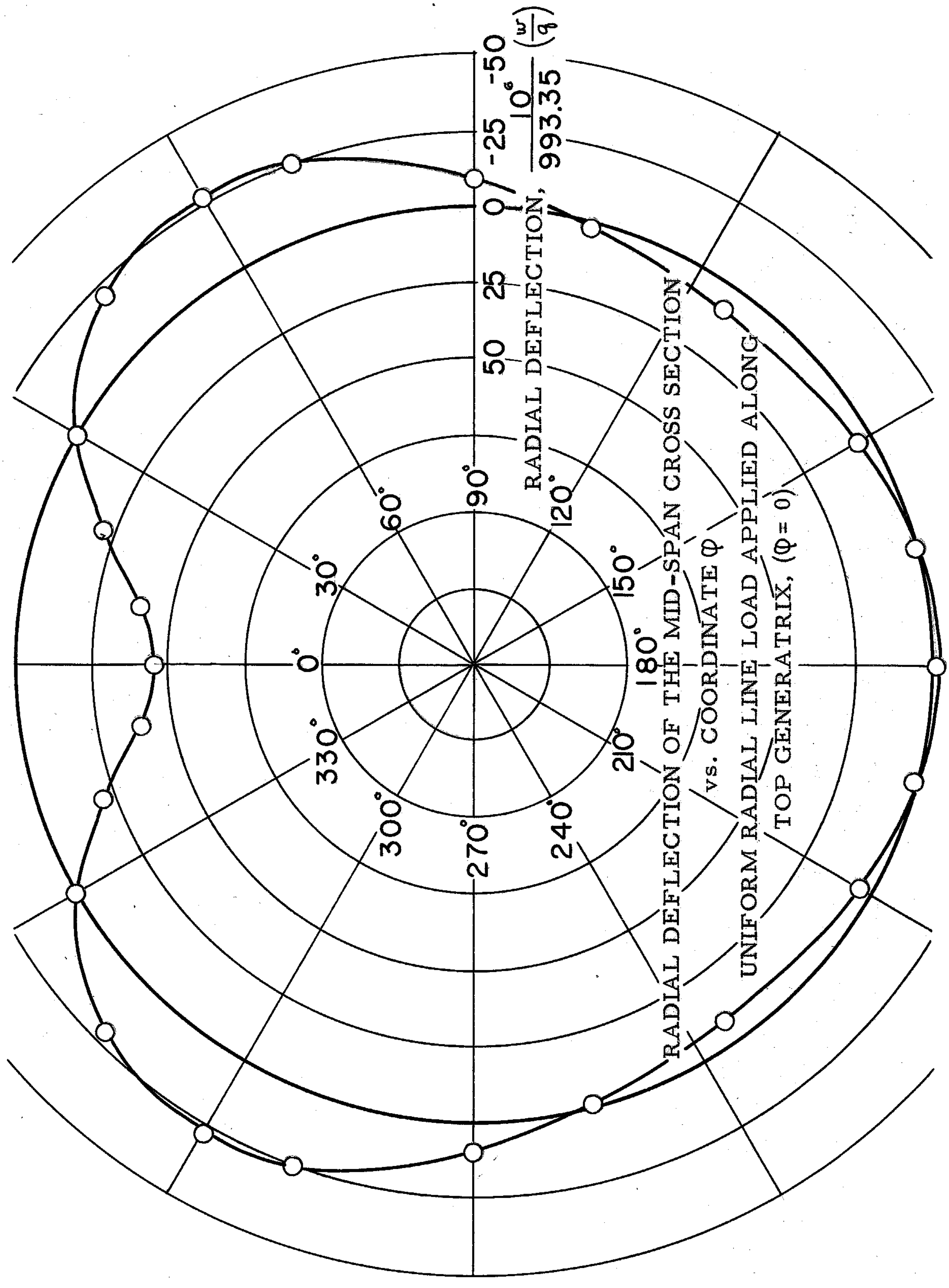
RADIAL DEFLECTION OF THE MID-SPAN CROSS SECTION
vs. COORDINATE φ
UNIFORM RADIAL LINE LOAD APPLIED ALONG
TOP GENERATRIX, (φ = 0)
RADIAL DEFLECTION, $\frac{10^{6}}{993.35}\left(\frac{w}{q}\right)$
-50
-25
0
25
50
0°
30°
60°
90°
120°
150°
180°
210°
240°
270°
300°
330°

Fig. 7

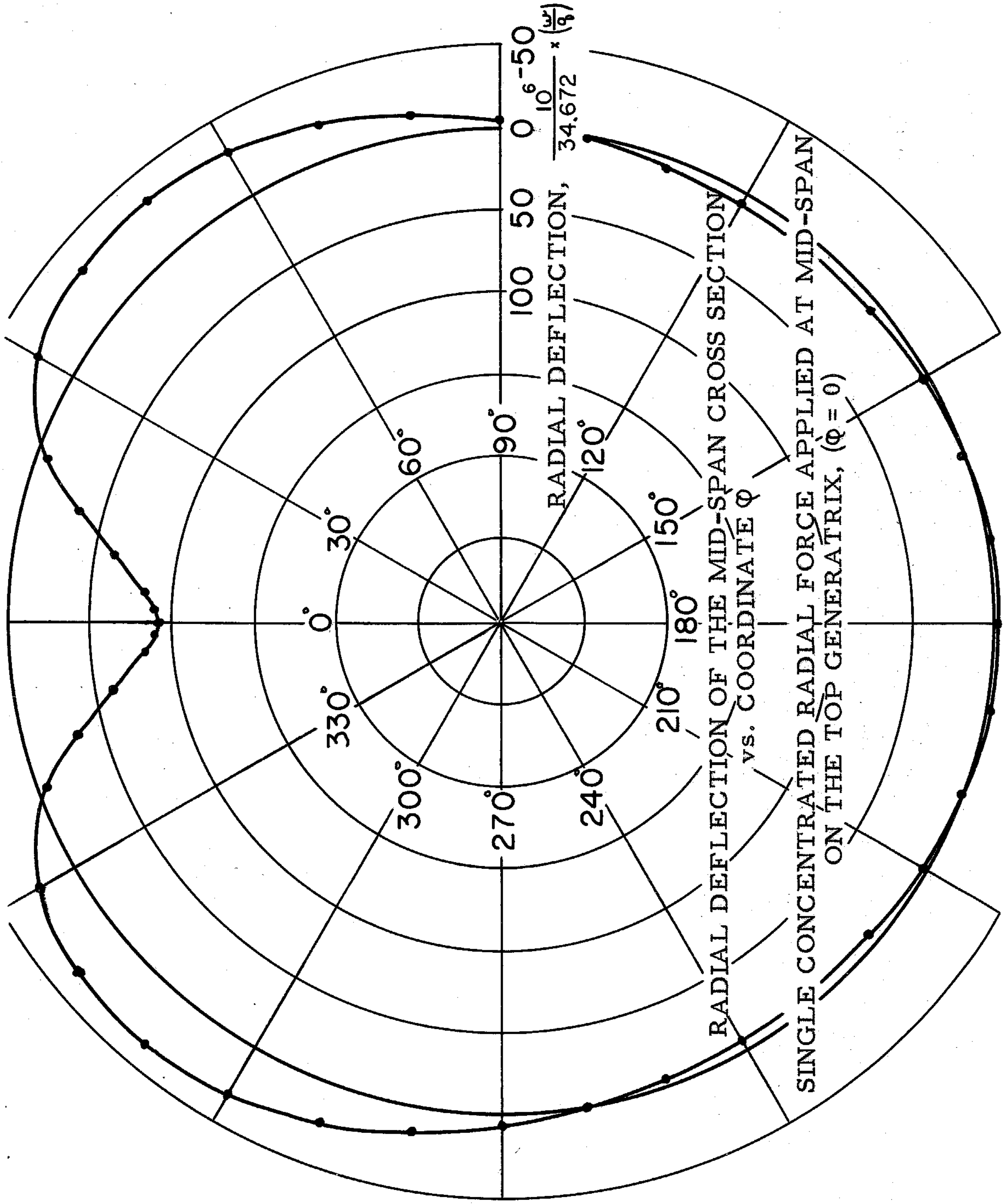
RADIAL DEFLECTION, $\frac{10^6}{34.672} \times \left(\frac{w}{q}\right)$
-50
0
50
100
0°
30°
60°
90°
120°
150°
180°
210°
240°
270°
300°
330°
RADIAL DEFLECTION OF THE MID-SPAN CROSS SECTION
vs. COORDINATE φ
SINGLE CONCENTRATED RADIAL FORCE APPLIED AT MID-SPAN
ON THE TOP GENERATRIX, (φ = 0)

Fig. 8

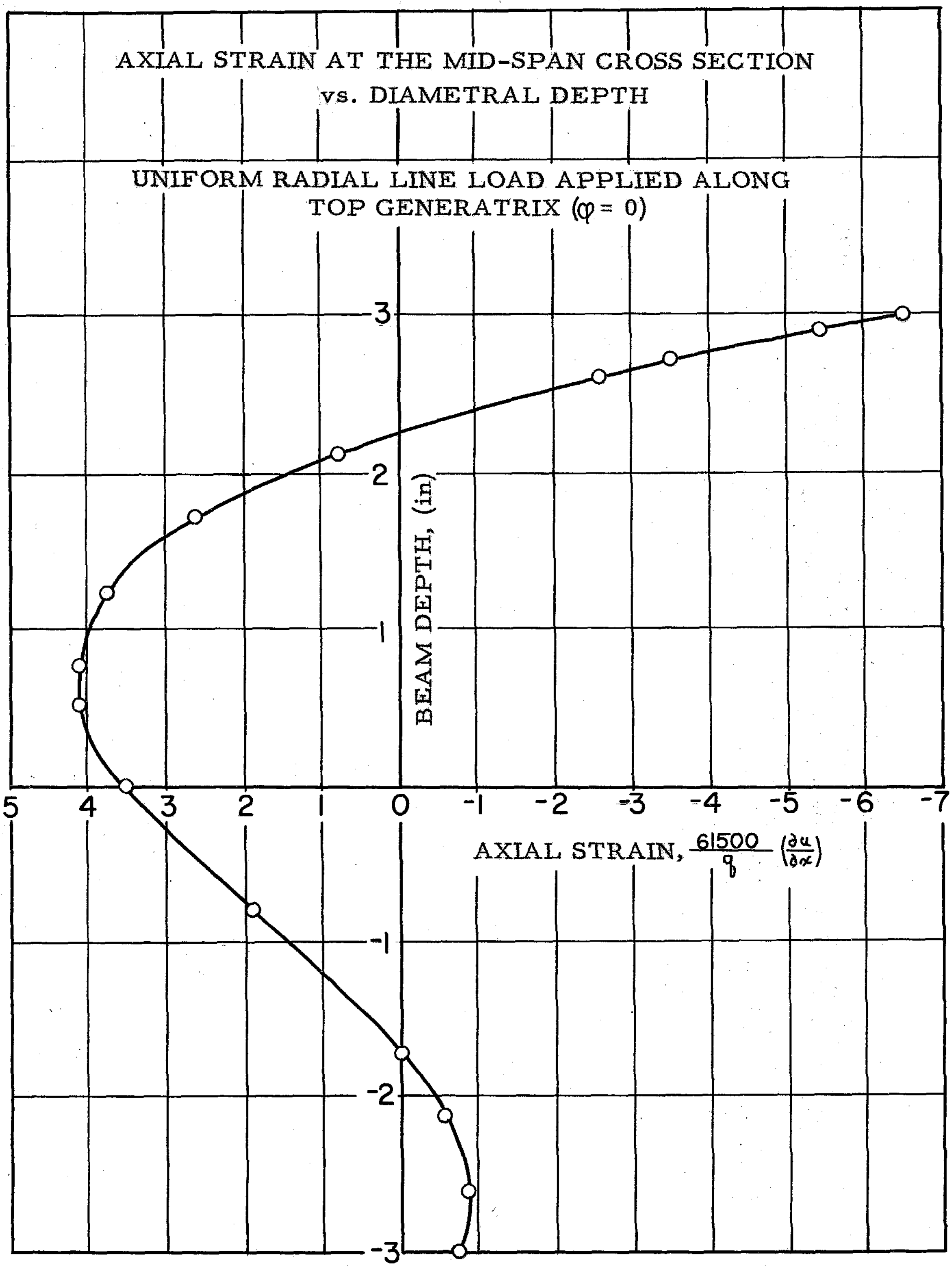

AXIAL STRAIN AT THE MID-SPAN CROSS SECTION
vs. DIAMETRAL DEPTH
UNIFORM RADIAL LINE LOAD APPLIED ALONG
TOP GENERATRIX ($\varphi = 0$)
BEAM DEPTH, (in)
3
2
1
-1
-2
-3
5
4
3
2
1
0
-1
-2
-3
-4
-5
-6
-7
AXIAL STRAIN, $\frac{61500}{q} \left(\frac{\partial u}{\partial x}\right)$

Fig. 9

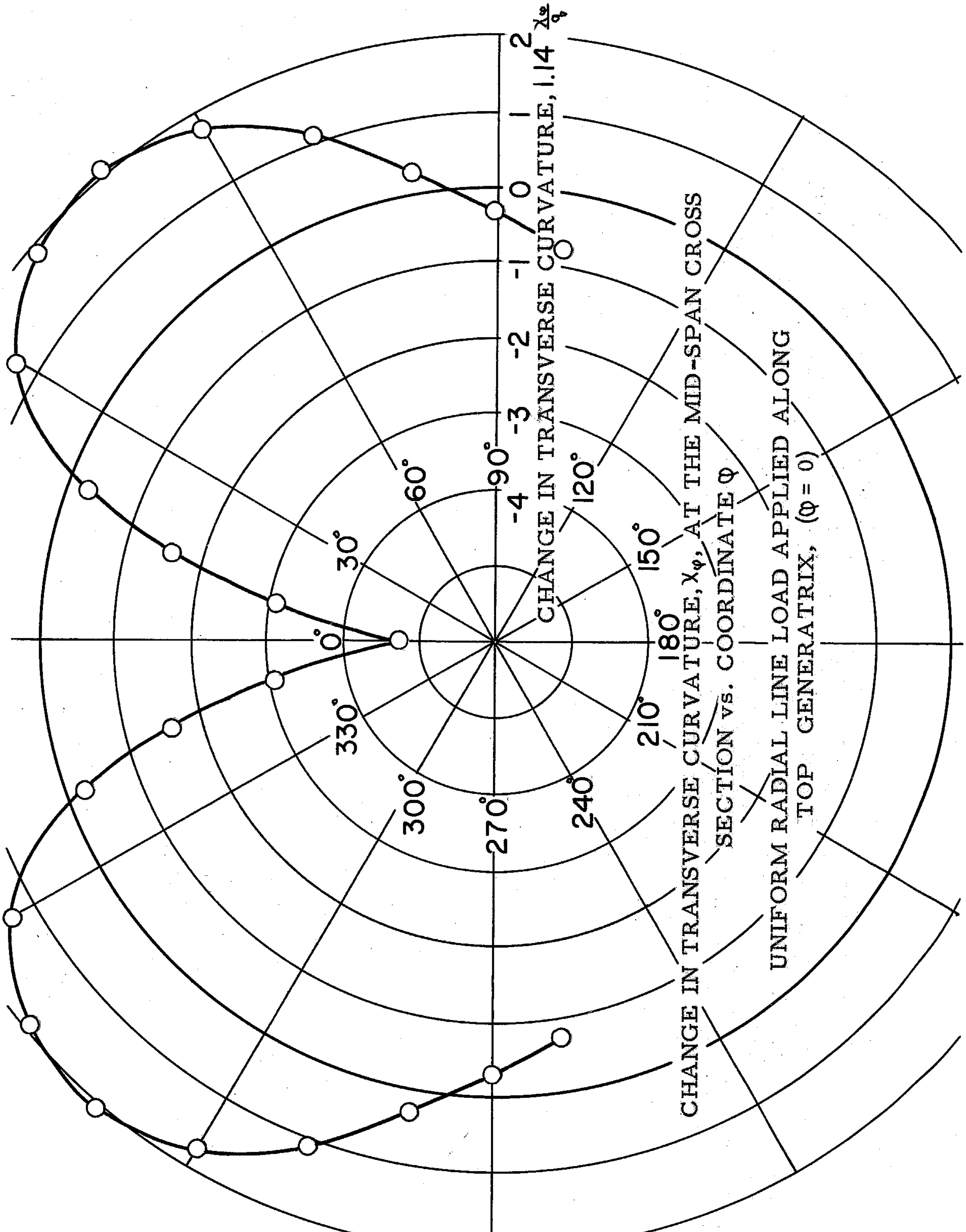
CHANGE IN TRANSVERSE CURVATURE, 1.14 $\frac{\chi_\varphi}{q_0}$
2
1
0
-1
-2
-3
-4
0°
30°
60°
90°
120°
150°
180°
210°
240°
270°
300°
330°
CHANGE IN TRANSVERSE CURVATURE, χ_φ, AT THE MID-SPAN CROSS SECTION vs. COORDINATE φ
UNIFORM RADIAL LINE LOAD APPLIED ALONG TOP GENERATRIX, ($\varphi = 0$)

Fig. 10

V. EXPERIMENTAL APPARATUS

A. Physical Description of the Cylinder

The cylindrical shell used in performing the experimental portion of this study is shown in Fig. 11. The length of the cylinder is 45 inches; the cross sectional diameter is 6.734 inches. The shell is made of sheet metal having a thickness of 0.015 inches. There is a welded axial seam which during the experiments was always located at a position of minimum extension and radial displacement so that it had a negligible effect upon the symmetry of the shell. A heavy transverse ring stiffener is brazed to each end of the cylinder. The cylinder is supported on four small (3/8 inch square) rubber pads directly under the ring stiffened ends of the cylinder. Fig. 5 shows schematically these four points of support.

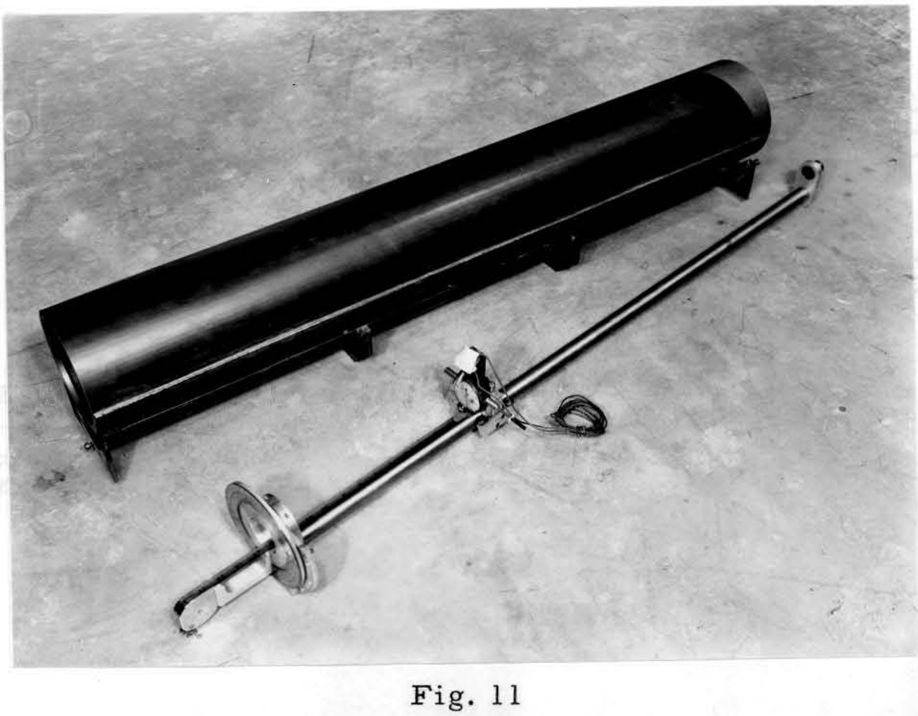

Fig. 11

B. Uniform Radial Line Loading Apparatus

To simulate the uniform radial line load use is made of a thin rubber strip and a ballast supporting wire net. The stripping is grooved and 3/8 inches wide as shown in Fig. 12, which furnishes flexibility in both the transverse and longitudinal directions. It is placed along the top generatrix ($\varphi = 0$) extending the full length of the cylinder. The ballast supporting net is 5 inches wide to accommodate the 25 pound ballast sacks, four of which are placed axially on the net extending the full length of the cylinder. The loading is thus not precisely a line load but is actually a 3/8" wide strip load. Fig. 13 shows the rubber stripping in place and the net and ballast sacks in the foreground.

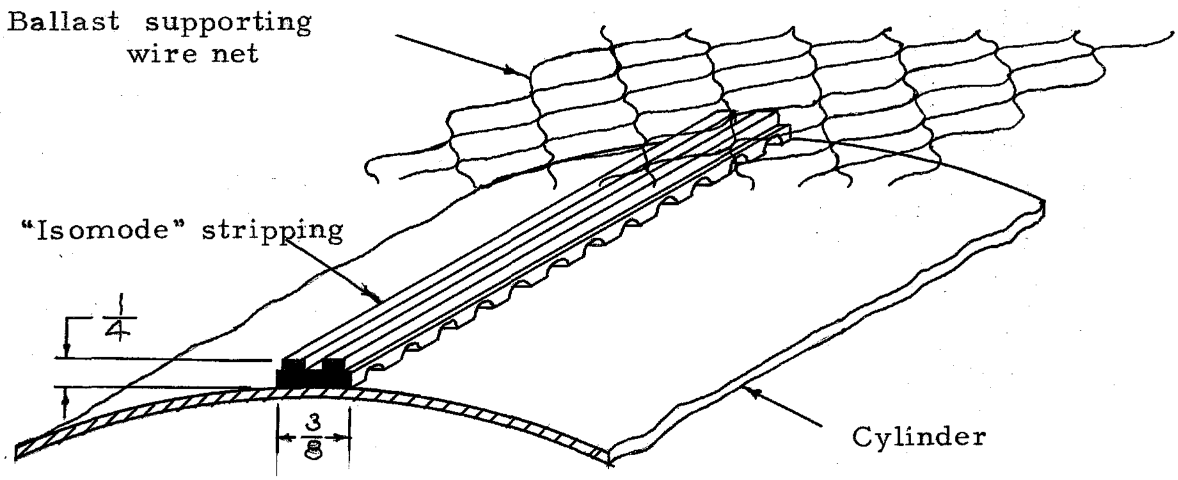

Fig. 12

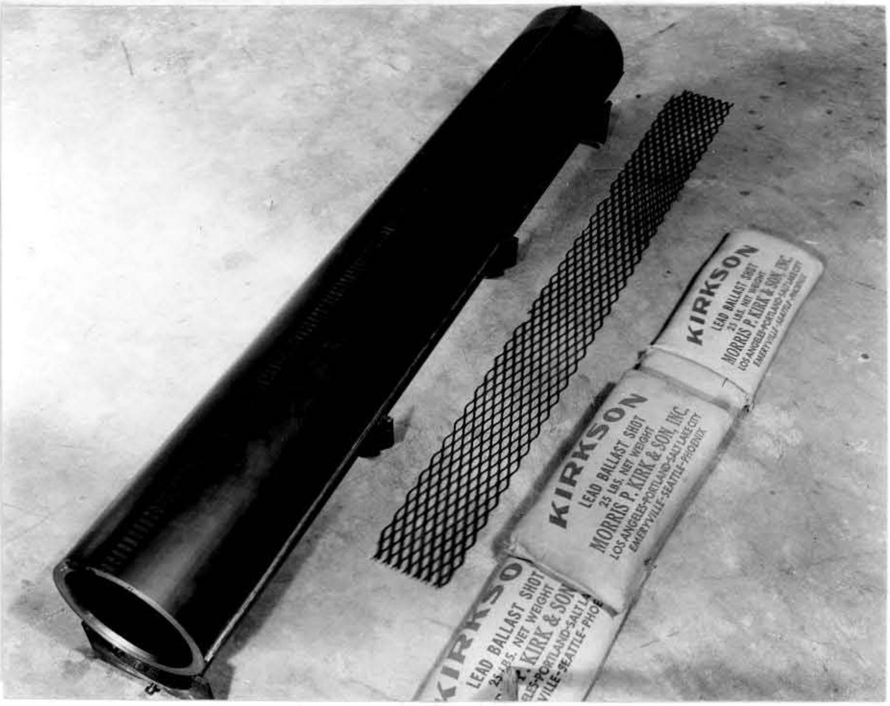

Fig. 13

C. Radial Concentrated Loading Apparatus

The radial concentrated force is applied by the apparatus shown in Fig. 14 which consists of a wooden fixture through which slides a 1/2 inch steel rod. The concentrated force is applied by the contact end of the rod which is slightly tapered and spherical.

D. Apparatus for Displacement Measurements

The radial measurements are obtained by introducing into the cylinder a 1-inch Ames dial gage ($\pm$ 0.001"). The gage is mounted on a small carriage which can slide along a full length of shaft which is in turn mounted at each end of the cylinder in suitable bearing. It is possible to position the dial gage at any desired point of the shell surface. Figure 15 shows in detail the Ames dial gage, its carriage mount, and an angle protractor to designate the position coordinate φ. The tape

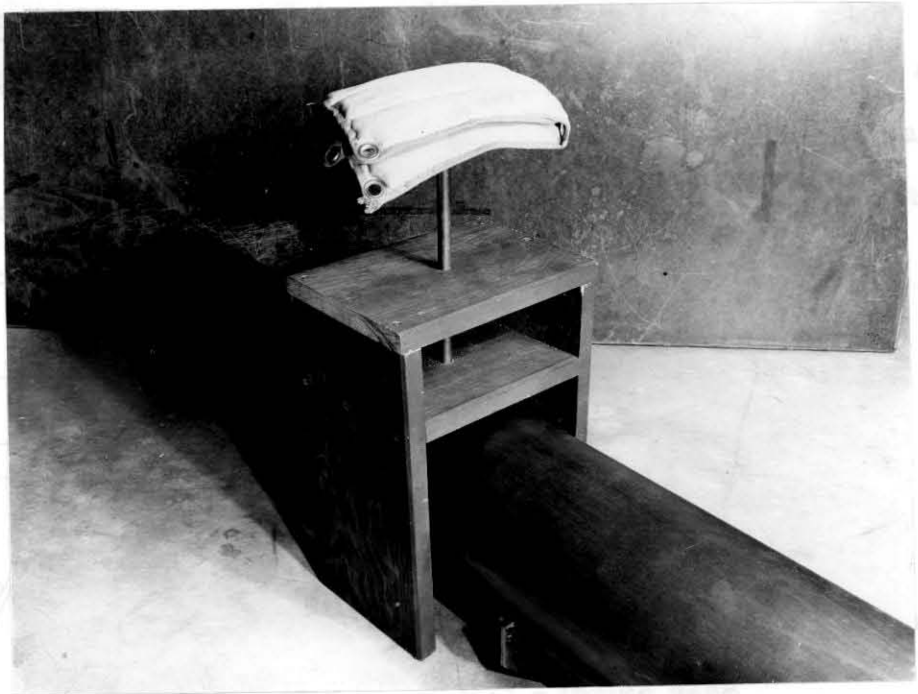

Fig. 14

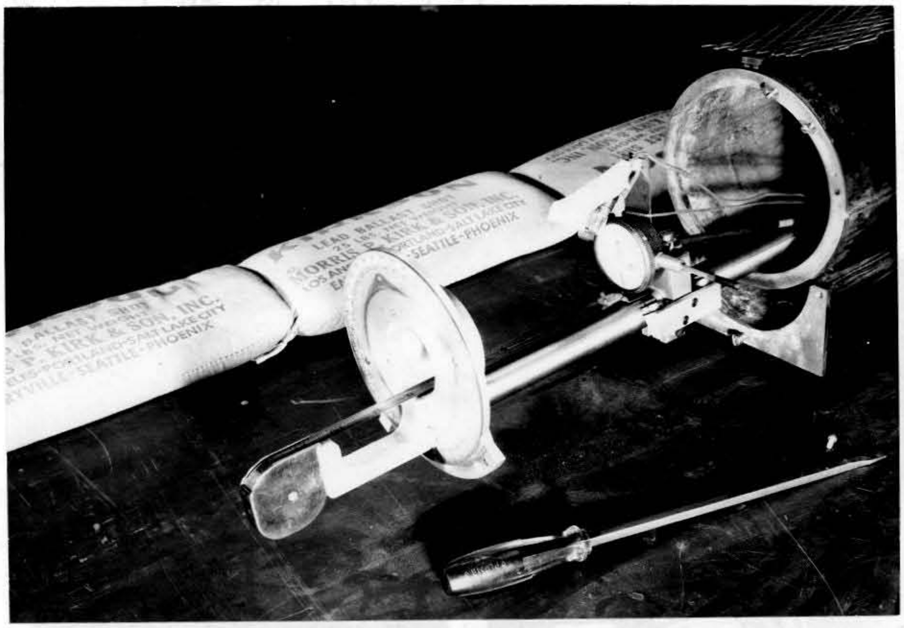

Fig. 15

measure, also shown in the figure, is to designate the axial position coordinate, α.

E. Strain Measurement Apparatus

Strain is measured with Type "A" SR4 wire strain gages attached to the shell surface with Duco household cement. The gages are located at the mid-span transverse cross section ($\alpha = 0$). Their positions on this cross section are shown in Fig. 16 and 17.

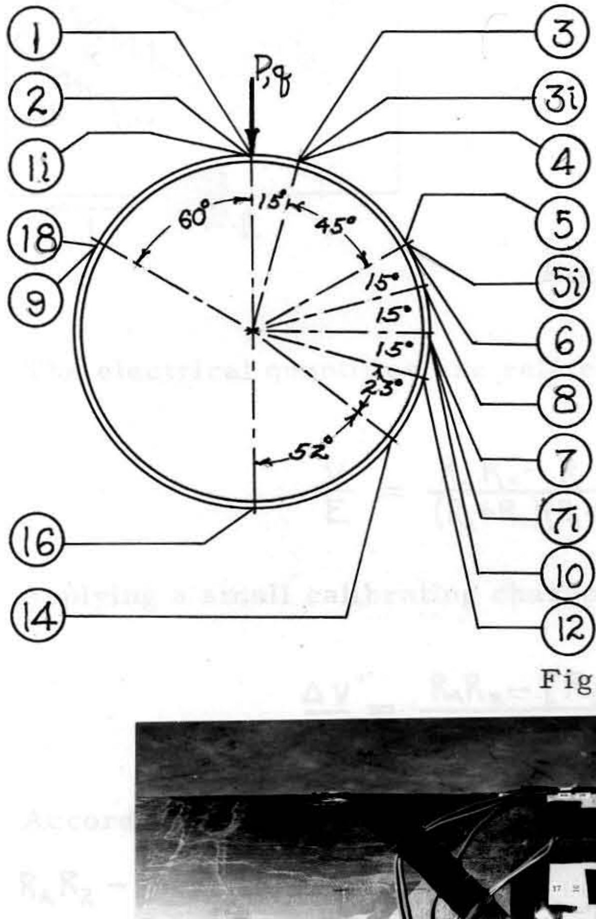

Even numbers - axial strain gage
Odd numbers - circumferential gage
i - Inside gage

Fig. 16

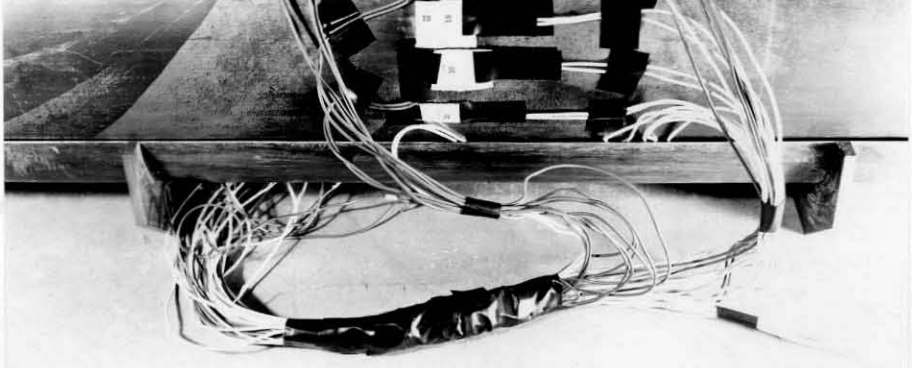

Fig. 17

The basic D.C. resistance bridge circuit to which each gage is associated is shown schematically in Fig. 18.

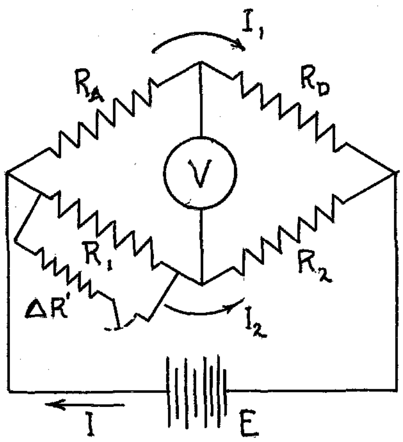

R_A = Active strain gage, 120 Ω
R_D = Dummy gage, 120 Ω
R_1, R_2 = Stationary bridge resistors
E = D. C. emf, 6 volts
$\Delta R'$ = Resistance calibrator

Fig. 18

The electrical quantities are related by the following expression:

$$\frac{V}{E} = \frac{R_A R_2 - R_1 R_D}{(R_A + R_D)(R_1 + R_2)} \tag{40}$$

Applying a small calibrating change in R_1, Eq. 40 becomes,

$$\frac{\Delta V'}{E} = \frac{R_A R_2 - [R_1 - \Delta R'] R_D}{(R_A + R_D)(R_1 + R_2 - \Delta R')} \tag{41}$$

According to the conjugate or balancing condition of the bridge, $R_A R_2 - R_1 R_D = 0$. Since $\Delta R'$ is small compared with R_1 and R_2, Eq. 41 may be expressed to a first order approximation, as

$$\frac{\Delta V'}{E} = \frac{\Delta R' R_D}{(R_A + R_D)(R_1 + R_2)} \tag{42}$$

Similarly, for a small change in R_A,

$$\frac{\Delta V}{E} = \frac{\Delta R_A R_2}{(R_A + R_D)(R_1 + R_2)} \tag{43}$$

Dividing Eq. 43 by Eq. 42, one obtains,

$$\frac{\Delta R_A}{R_A} = \left\{ \frac{1}{R_2} \frac{\Delta R'}{\Delta V'} \right\} \Delta V = K \, \Delta V \tag{44}$$

where K is the calibration constant. The gage factor, G.F., relates the percentage change in resistance to the unit surface strain and is defined by,

$$\epsilon = \frac{1}{G.F.} \frac{\Delta R_A}{R_A} \tag{45}$$

A Brown electronic continuous balance potentiometer and a multi-stage switch are employed and are shown in Fig. 19.

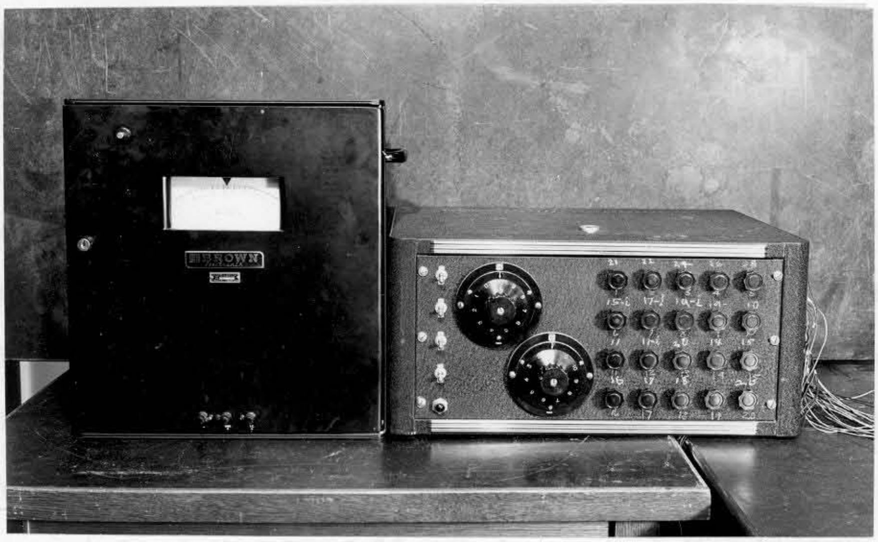

Fig. 19

VI. EXPERIMENTAL PROCEDURE

A. Radial Deflection Measurements

Before the application of loads to the cylinder, an initial survey of the mid-span transverse cross section is made. Final surveys are made of the cross section for the cylinder in the loaded conditions. The difference between the final and initial surveys is then the net radial deflection resulting from the applied loads. The cross section in the initial survey deviates irregularly about a mean circle. The maximum deviations from this mean circle are 0.06 inches. It was verified that these deviations had a negligible effect upon the stresses and strains, or in other words, the magnitude of the stress was well below that required for local buckling.

An approximately uniform radial line load, extending the full length of the cylinder along the top generatrix, is applied by the apparatus described previously. The measured average line load intensity, q, is 2.53 pounds per inch. This loading causes a 0.11 inch maximum radial deflection at mid-span directly under the load. Fig. 20 shows the experimental data for the radial deflections at the mid-span. A curve of the computed solution for 2.53 pounds per inch line load intensity is also shown.

For the second type of load, a single radial concentrated force of 22 pounds is applied at the mid-span by means of the fixture previously described (Fig. 14). Fig. 21 shows the experimental data for the radial deflections at the mid-span as a result of this concentrated load. A curve of the computed displacements for a force of 22 pounds is also shown.

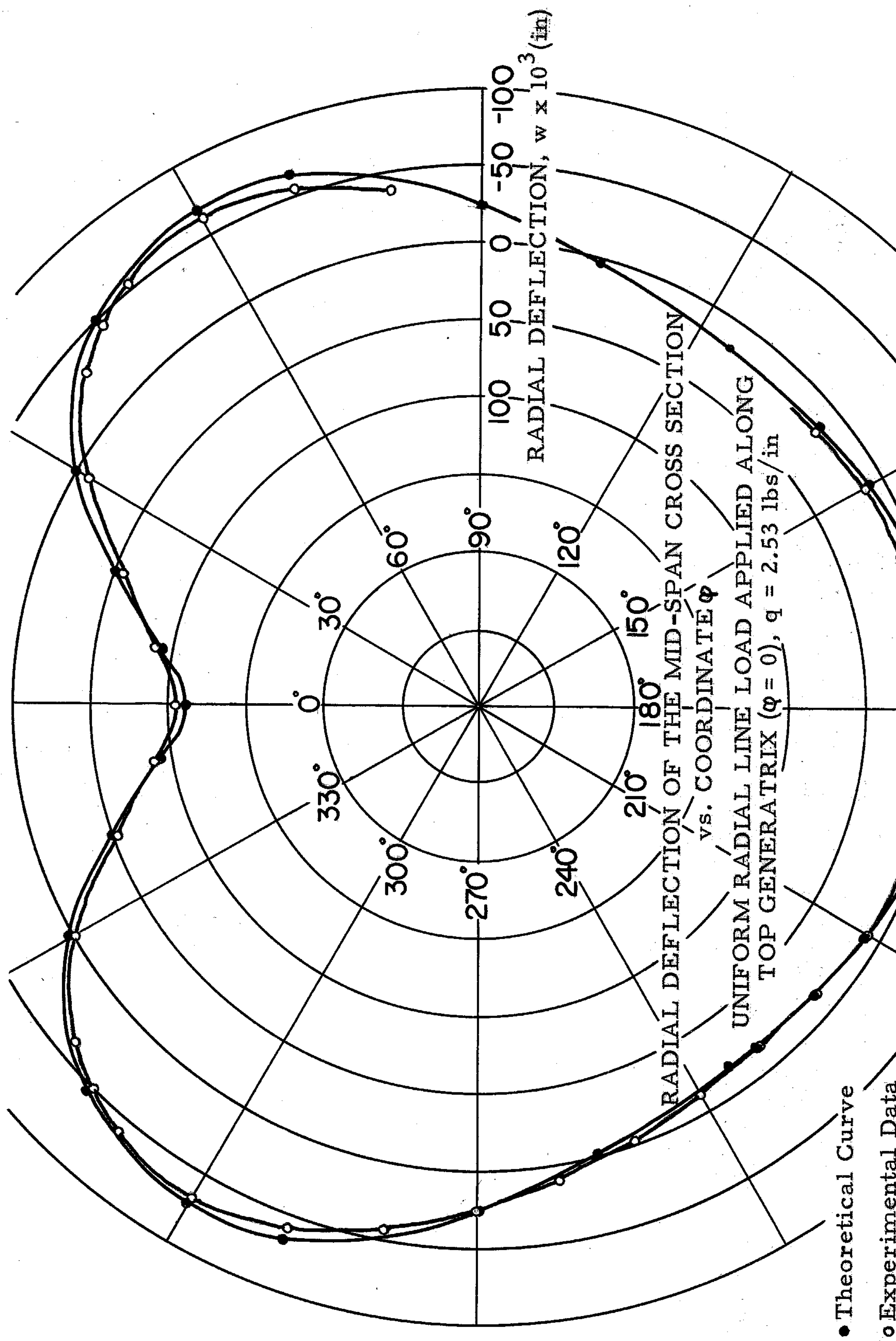
RADIAL DEFLECTION, w x 10^3 (in)
100
50
0
-50
-100
0°
30°
60°
90°
120°
150°
180°
210°
240°
270°
300°
330°
RADIAL DEFLECTION OF THE MID-SPAN CROSS SECTION
vs. COORDINATE φ
UNIFORM RADIAL LINE LOAD APPLIED ALONG
TOP GENERATRIX (φ = 0), q = 2.53 lbs/in
• Theoretical Curve
o Experimental Data

Fig. 20

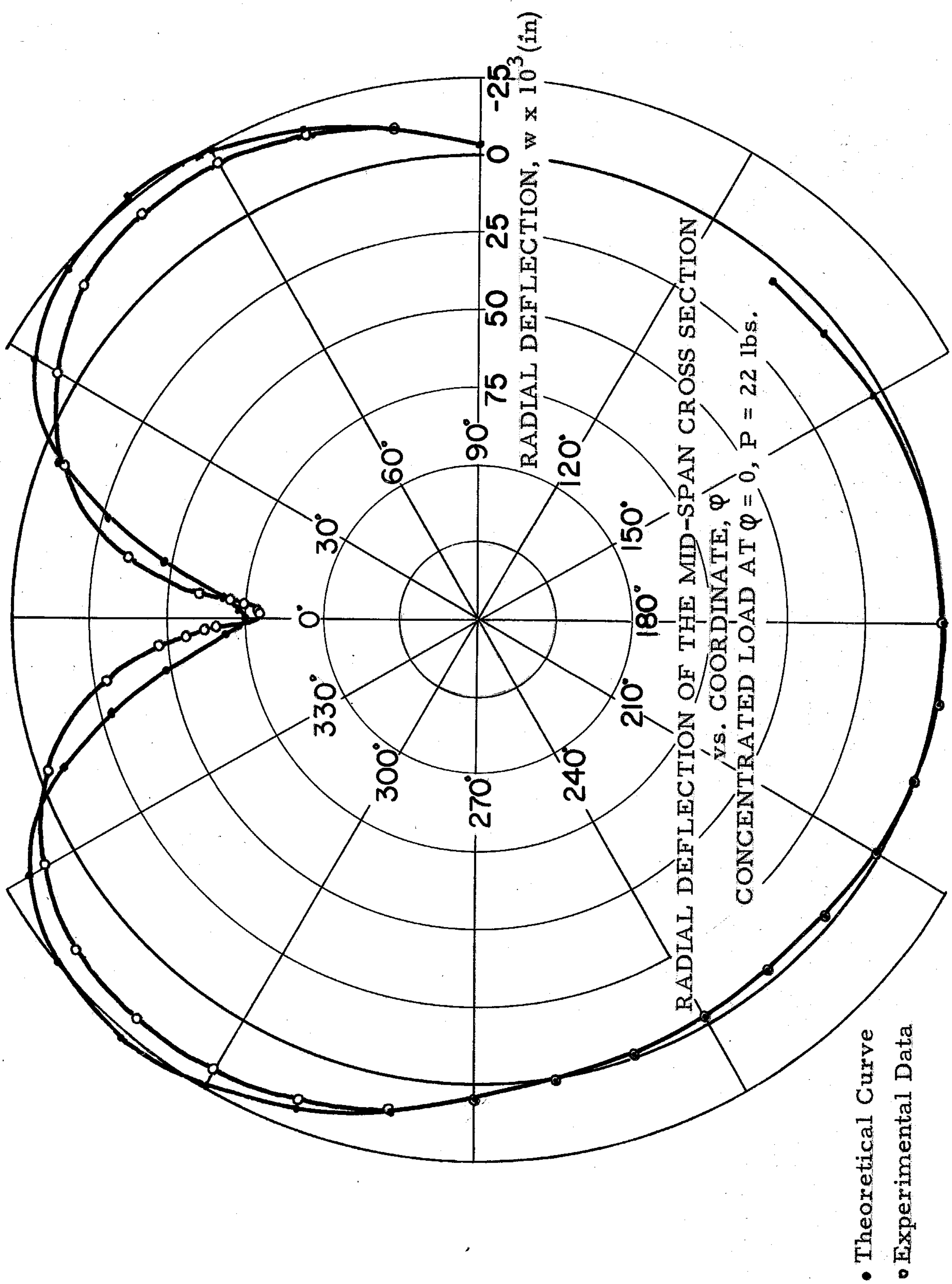
RADIAL DEFLECTION, w x 10^3 (in)
-25
0
25
50
75
0°
30°
60°
90°
120°
150°
180°
210°
240°
270°
300°
330°
RADIAL DEFLECTION OF THE MID-SPAN CROSS SECTION
vs. COORDINATE, φ
CONCENTRATED LOAD AT φ = 0, P = 22 lbs.
• Theoretical Curve
o Experimental Data

Fig. 21

The computed solution for the radial deflections at the mid-span produced by the radial concentrated load agrees less closely (within 33 percent at positions of maximum Ames dial gage readings) with the experimental results than in the case of the uniform line load. This discrepancy is partly due to the fact that an insufficient number of terms were used in the computations and is partly due to the fact that the analysis is not applicable in the immediate vicinity of the applied force where $\gamma_{x\varphi}$ and ϵ_z are not negligible.

B. Measurement of Strains Caused by the Uniform Radial Line Load

Axial surface strains ϵ_x are measured at nine locations around the mid-span transverse cross section (Fig. 16). Since with this type of loading there is negligible axial plate bending the axial surface strain is the same as the axial middle surface strain. Figure 22 shows the measured axial outside surface strains at the mid-span, and a curve of the computed middle surface axial strain ϵ_1 is also shown for the same cross section.

Transverse surface strains ϵ_φ are measured at four locations around the mid-span transverse cross section. At these four positions, gages are attached both on inside and outside surfaces of the shell. This is to facilitate the separate determination of the direct extension and the transverse bending strains. In the analysis, the direct circumferential extension of the middle surface ϵ_2 is neglected. At the position of maximum gage reading, directly below the load 7 percent of the reading is due to the effect of direct circumferential extension of the middle surface. Thus, this effect, although present, is small. Fig. 23 shows the experimental data for the transverse outside surface strains resulting from transverse bending. With this data, is included a curve

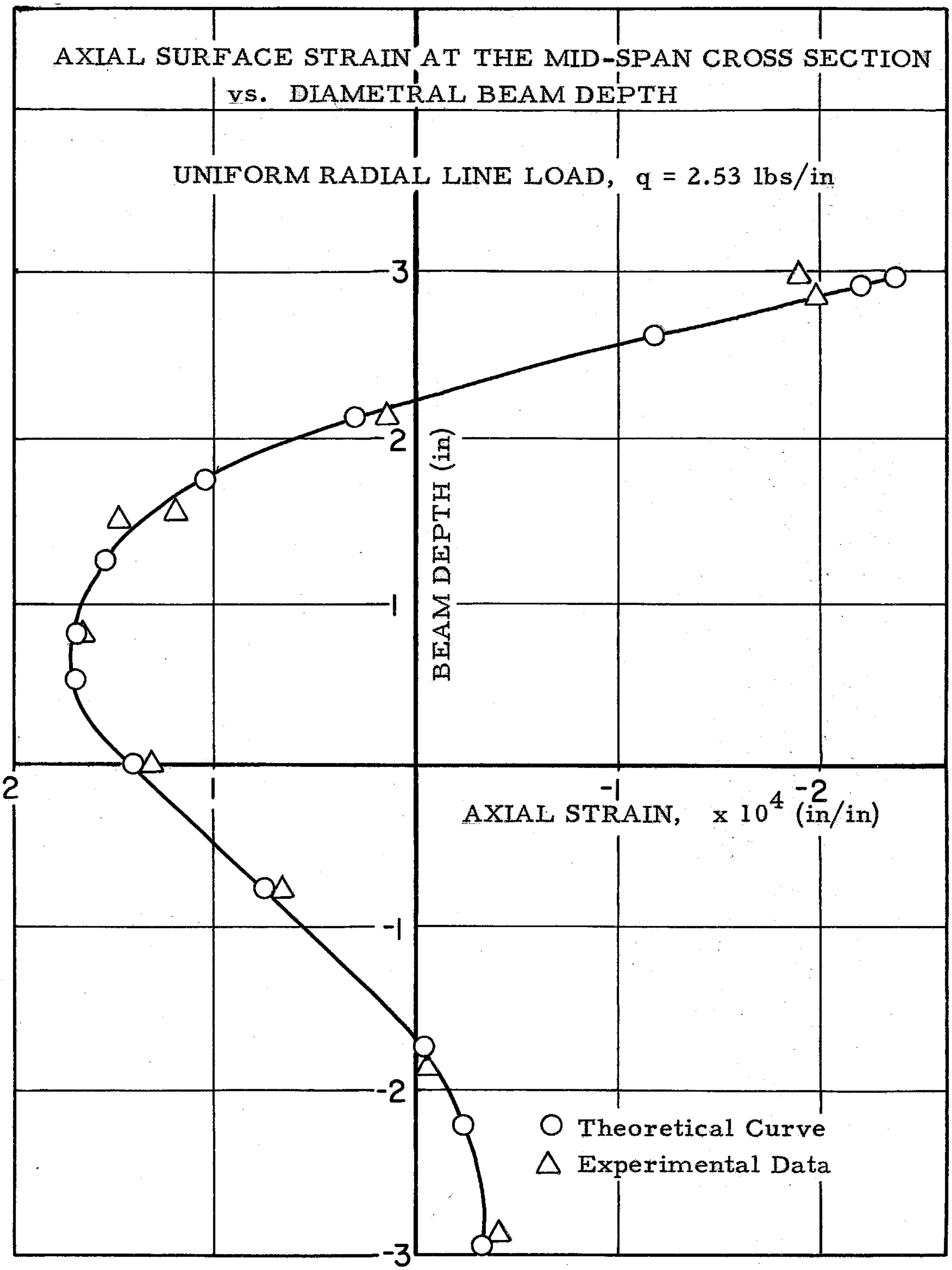
AXIAL SURFACE STRAIN AT THE MID-SPAN CROSS SECTION
vs. DIAMETRAL BEAM DEPTH
UNIFORM RADIAL LINE LOAD, q = 2.53 lbs/in
3
2
1
-1
-2
-3
BEAM DEPTH (in)
2
1
-1
-2
AXIAL STRAIN, x 10⁴ (in/in)
Theoretical Curve
Experimental Data

Fig. 22

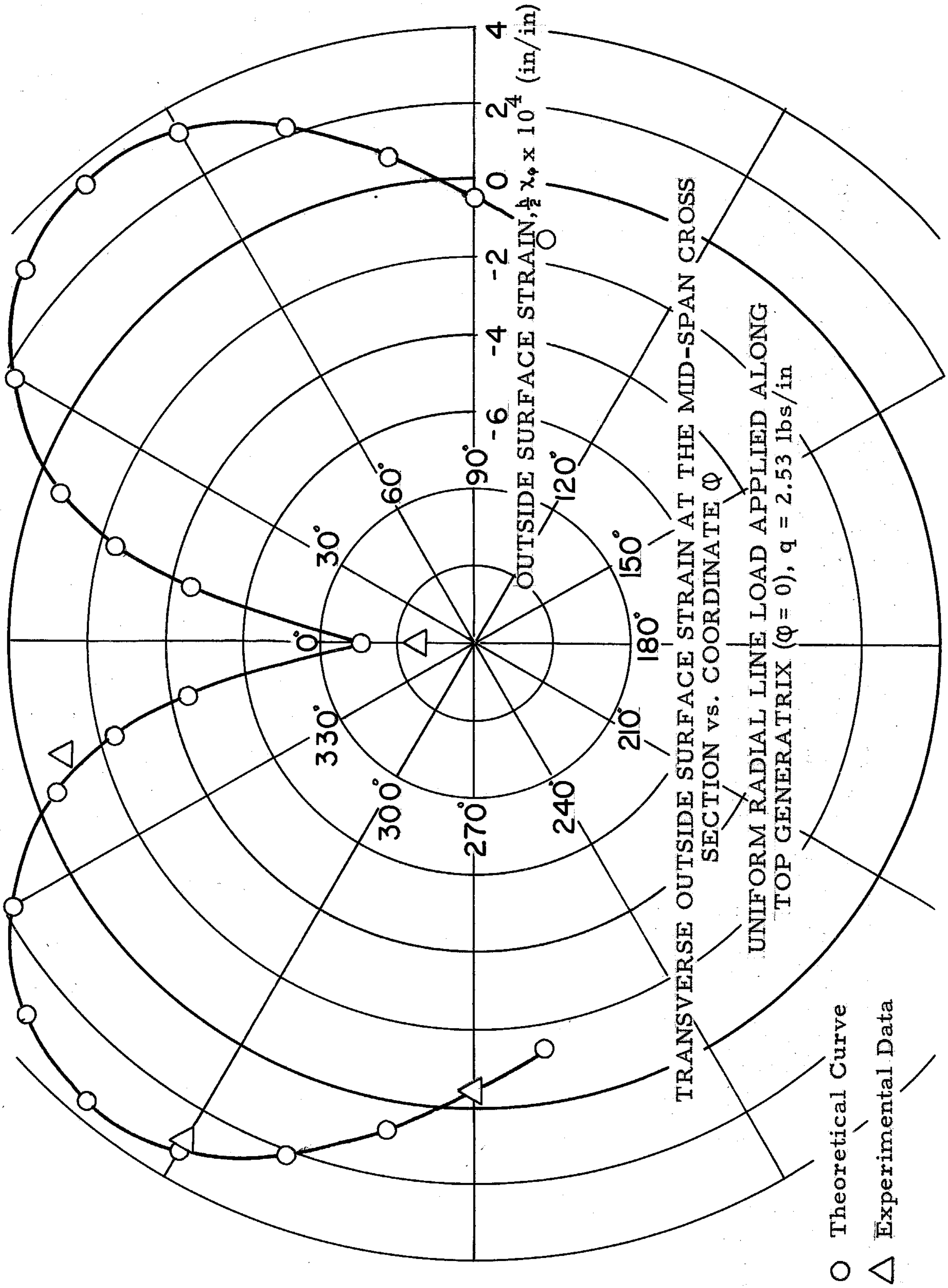
TRANSVERSE OUTSIDE SURFACE STRAIN AT THE MID-SPAN CROSS SECTION vs. COORDINATE φ
UNIFORM RADIAL LINE LOAD APPLIED ALONG TOP GENERATRIX (φ = 0), q = 2.53 lbs/in
OUTSIDE SURFACE STRAIN, $\frac{h}{2}\chi_\phi \times 10^4$ (in/in)
4
2
0
-2
-4
-6
0°
30°
60°
90°
120°
150°
180°
210°
240°
270°
300°
330°
○ Theoretical Curve
△ Experimental Data

Fig.23

of the computed solution for the outside transverse surface strain, $\frac{h}{2}\chi_{\varphi}$.

VII. COMPARISON OF THEORY AND EXPERIMENT

The agreement between computed and experimental results depends on the number of terms included in the evaluation of the series expressions for the deflections, etc. as well as on the accuracy of the experimental data.

The measured radial deflections are estimated to be accurate to ± 0.003 inches. This represents the combined error accumulated from the initial and final radial deflection surveys. Considering the line load case,'the computed solution for the radial deflection at the mid-span cross section checks very closely with observation (within 4 percent at positions of maximum Ames dial gage readings). From the convergence properties of the series expressions (see example calculations, page 19), for these deflections, agreement within 5 percent of the measured results would be obtained if terms are included only through the fifth transverse harmonic ($n = 5$), and through the fifth axial harmonics, ($m = 5$). Therefore satisfactory results, for most practical applications, can be obtained with an appreciable reduction in the numerical computations from what was actually used.

Considering the possible SR4 strain gage accuracy and that of the associated equipment, strain measurements are estimated to be accurate to 5 percent. The computed solution for the axial surface strain, $\frac{\partial u}{\partial x}$, and transverse surface strain, $\frac{h}{2}\chi_{\varphi}$, of the mid-span cross section due to the uniform radial line load checks very closely with observation.

See Figs. 22 and 23. An estimate of the experimental scatter and/or asymmetry of the strains is obtained by comparing measured strains for a group of gages which are located symmetrically and therefore strained the same amount theoretically. The difference in strain values recorded at these locations does not exceed 3.5 percent of the readings. The correlation of the axial strain, $\frac{\partial u}{\partial x}$. with the experimental data is within 10 percent of the maximum gage readings except in a 30° region about the load. The 0.05×10^{-3} inch per inch maximum discrepancy in axial strain measurement in this region is attributed to the fact that the loading was actually applied over a width of 3/8" instead of the zero inches used in the computations. In this region, also, it is found that maximum discrepancies occur for the transverse surface strain measurements.

On the whole, the agreement between theory and experiment is satisfactory and it is concluded that the simplified analysis gives accurate values for the stresses and deflections for thin-walled cylinders with sufficiently large ratios of span to radius except in the vicinity of a concentrated load, etc.

VIII. SUMMARY AND CONCLUSIONS

A simplified method of analysis of a laterally loaded thin-walled cylinder is developed. It is based on neglecting the effects of shear strain and circumferential strain. When the ratio of length to radius of the cylinder is sufficiently large and the ratio of wall thickness to radius sufficiently small, for most types of lateral loadings, these strains have small effects on the state of stress. However, the analysis is not valid in the vicinity of concentrated forces and in local regions near abrupt changes in load intensity, where the circumferential and shear strains are not negligible.

Stresses and displacements are calculated for a simply supported cylinder with a radial concentrated force at the mid-span section and also the case with the uniform radial line load extending along the top generatrix.

Distortions of the mid-span cross section are measured experimentally. In the case of the line load, the radial deflections are found to agree within 4 percent at positions of maximum Ames dial gage readings. A similar degree of accuracy is obtained for the case of the radial concentrated force except in a local region near the force.

Stresses are measured on a cylinder with a uniform radial line load. The axial and circumferential stress distributions around the mid-span cross section are found to agree within 10 percent of the maximum gage readings except in a 30° local region near the load.

It is concluded that the simplified analysis gives accurate values of stresses and deflections for thin-walled cylinders having sufficiently large ratios of length to radius except in the vicinity of concentrated forces or near abrupt changes in load intensity.

APPENDIX A

Calculations

AXIAL STRAIN AT THE MID-SPAN TRANSVERSE CROSS SECTION FOR THE UNIFORM LINE LOAD

$$\frac{0.0613}{q}\frac{\partial u}{\partial x}=\sum_{m,n}^{\infty}\frac{\cos n\varphi \sin\frac{m\pi}{2}}{m^3 n^2\left[\frac{10^6}{n^4}+595.33\left(\frac{1-n^2}{m^2}\right)^2+46.05\left(\frac{n}{m}\right)^2\right]}$$

TABLE 3. TRANSVERSE HARMONIC CONTRIBUTIONS TO THE AXIAL STRAIN

A. First harmonic, $n = 1$.

$$\frac{0.0613\times 10^6}{q}\frac{\partial u}{\partial x}=\cos\varphi\sum_{m}^{\infty}\frac{\sin\frac{m\pi}{2}}{m^3}$$

m	m^3	$\Sigma^{-1}\times 10^6$
1	1	+1.000
3	27	− .037
5	125	+ .008
7	343	− .003
9	729	+ .001
		0.999

B. Second harmonic, $n = 2$

$$\frac{0.0613}{q}\frac{\partial u}{\partial x}=\cos 2\varphi\left(\frac{1}{4}\right)\sum_{m}^{\infty}\frac{\sin\frac{m\pi}{2}}{62506\,m^3+104\,m+5358\,m^{-1}}$$

m	m^3	$62{,}506m^3$	$104m$	m^{-1}	$5{,}358m^{-1}$	Σ	$\frac{1}{4}\Sigma^{-1}\times 10^6$
1	1	62,506	104	1.000	5,358	67,968	+14.712
3	27	1,687,662	312	.333	1,784	1,689,758	− .592
5	125	7,813,250	520	.200	1,072	7,814,842	+ .137
7	343	21,439,558	728	.143	766	21,441,052	− .047
9	729	45,566,874	936	.111	595	45,568,405	+ .022
11	1,331	83,195,486	1,144	.091	488	83,197,118	− .012
13	2,197	137,325,682	1,351	.077	413	137,327,447	+ .007
15	3,375	210,957,750	1,560	.067	359	210,959,669	− .005
17	4,913	307,091,978	1,768	.059	316	307,094,062	+ .003
19	6,859	428,728,654	1,976	.053	284	428,730,914	− .002
21	9,261	578,868,066	2,184	.048	257	578,870,507	+ .002
							3.56

C. Third harmonic, $n = 3$.

$$\frac{0.0613}{g}\,\frac{\partial u}{\partial x} = \cos 3\varphi \left(\frac{1}{9}\right) \sum_{m}^{\infty} \frac{\sin \frac{m\pi}{2}}{12{,}352\, m^3 + 328\, m + 38{,}101\, m^{-1}}$$

m	m^3	m^{-1}	$12{,}352m^3$	$328m$	$38{,}101m^{-1}$	Σ	$\frac{1}{9}\Sigma^{-1} \times 10^6$
1	1	1.000	12,352	328	38,101	50,781	+19.692
3	27	.333	333,504	984	12,688	347,176	− 2.880
5	125	.200	1,544,000	1,640	7,620	1,553,260	+ .644
7	343	.143	4,236,736	2,296	5,448	4,244,480	− .236
9	729	.111	9,004,608	2,952	4,229	9,011,789	+ .111
11	1,331	.091	16,440,512	3,608	3,467	16,447,587	− .061
13	2,197	.077	27,137,344	4,264	2,934	27,144,542	+ .037
15	3,375	.067	41,688,000	4,920	2,553	41,695,473	− .024
17	4,913	.059	60,685,376	5,576	2,248	60,693,200	+ .017
19	6,859	.053	84,722,368	6,232	2,019	84,730,619	− .012
21	9,261	.048	114,391,872	6,888	1,829	114,400,589	+ .009
23	12,167	.044	150,286,784	7,544	1,676	150,296,004	− .007
25	15,625	.040	193,000,000	8,200	1,524	193,009,724	+ .005
27	19,683	.037	243,124,416	8,856	1,410	243,134,682	− .004
29	24,389	.035	301,252,928	9,512	1,334	301,263,774	+ .003
31	29,791	.032	367,978,432	10,168	1,219	367,989,819	− .003
33	35,937	.030	443,893,824	10,824	1,143	443,905,791	+ .002
35	42,875	.029	529,592,000	11,480	1,105	529,604,585	− .002
37	50,653	.027	625,665,856	12,136	1,029	625,679,021	+ .001
							1.92

D. Fourth harmonic, $n = 4$.

$$\frac{0.0613}{q^*}\frac{\partial u}{\partial x} = \cos 4\varphi\left(\frac{1}{16}\right)\sum_{m}^{\infty} \frac{\sin \frac{m\pi}{2}}{3912m^3 + 648m + 133{,}949m^{-1}}$$

m	m^3	m^{-1}	$3{,}912m^3$	$648m$	$133{,}949m^{-1}$	Σ	$\frac{1}{16}\Sigma^{-1} \times 10^6$
1	1	1.000	3,912	648	133,949	138,509	+7.220
3	27	.333	105,624	1,944	44,605	152,173	−6.571
5	125	.200	489,000	3,240	26,790	519,030	+1.927
7	343	.143	1,341,816	4,536	19,155	1,365,507	− .732
9	729	.111	2,851,848	5,832	14,868	2,872,548	+ .348
11	1,331	.091	5,206,872	7,128	12,189	5,226,189	− .191
13	2,197	.077	8,594,664	8,424	10,314	8,613,402	+ .116
15	3,375	.067	13,203,000	9,720	8,975	13,221,695	− .076
17	4,913	.059	19,219,656	11,016	7,903	19,238,585	+ .052
19	6,859	.053	26,832,408	12,312	7,099	26,851,819	− .037
21	9,261	.048	36,229,032	13,608	6,430	36,249,070	+ .028
23	12,167	.044	47,597,304	14,904	5,894	47,618,102	− .021
25	15,625	.040	61,125,000	16,200	5,358	61,146,558	+ .016
27	19,683	.037	76,999,896	17,496	4,956	77,022,348	− .013
29	24,389	.035	95,409,768	18,792	4,688	95,433,248	+ .011
31	29,791	.032	116,542,392	20,088	4,286	116,566,766	− .009
33	35,937	.030	140,585,544	21,384	4,019	140,610,947	+ .007
35	42,875	.029	167,727,000	22,680	3,885	167,753,565	− .006
37	50,653	.027	198,154,536	23,976	3,617	198,182,129	+ .005
39	59,319	.026	232,055,928	25,272	3,483	232,084,683	− .004
41	68,921	.024	269,618,952	26,568	3,215	269,648,735	+ .004
43	79,507	.023	311,031,384	27,864	3,081	311,062,329	− .003
45	91,125	.022	356,481,000	29,160	2,947	356,513,107	+ .003
47	103,823	.021	406,155,576	30,456	2,813	406,188,845	− .002
49	117,649	.020	460,242,588	31,752	2,679	460,277,319	+ .002
51	132,651	.020	518,930,712	33,048	2,679	518,966,439	− .002
53	148,877	.019	582,406,824	34,344	2,545	582,443,713	+ .002
55	166,375	.018	650,859,000	35,640	2,411	650,897,051	− .001
							0.13

E. Fifth harmonic, $n = 5$

$$\frac{0.0613}{q}\frac{\partial u}{\partial x} = \cos 5\varphi\left(\frac{1}{25}\right)\sum_{m}^{\infty}\frac{\sin\frac{m\pi}{2}}{1{,}606m^3 + 1{,}602\,m + 342{,}909m^{-1}}$$

m	m^3	m^{-1}	$1{,}606m^3$	$1{,}602m$	$342{,}909m^{-1}$	Σ	$\frac{1}{25}\Sigma^{-1} \times 10^6$
1	1	1.000	1,606	1,602	342,909	346,117	+2,889
3	27	.333	43,362	4,806	114,189	162,357	−6.159
5	125	.200	200,750	8,010	68,582	277,342	+3.606
7	343	.143	550,858	11,214	49,036	611,108	−1.636
9	729	.111	1,170,774	14,418	38,063	1,223,255	+ .817
11	1,331	.091	2,137,586	17,622	31,205	2,186,413	− .457
13	2,197	.077	3,528,382	20,826	26,404	3,575,612	+ .280
15	3,375	.067	5,420,250	24,030	22,975	5,467,255	− .183
17	4,913	.059	7,890,278	27,234	20,232	7,937,744	+ .126
19	6,859	.053	11,015,554	30,438	18,174	11,064,166	− .090
21	9,261	.048	14,873,166	33,642	16,460	14,923,268	+ .067
23	12,167	.044	19,540,202	36,846	15,088	19,592,136	− .051
25	15,625	.040	25,093,750	40,050	13,716	25,147,516	+ .040
27	19,683	.037	31,610,898	43,254	12,688	31,666,840	− .032
29	24,389	.035	39,168,734	46,458	12,002	39,227,194	+ .026
31	29,791	.032	47,844,346	49,662	10,973	47,904,981	− .021
33	35,937	.030	57,714,822	52,866	10,287	57,777,975	+ .017
35	42,875	.029	68,857,250	56,070	9,944	68,923,264	− .015
37	50,653	.027	81,348,718	59,274	9,259	81,417,251	+ .012
39	59,319	.026	95,266,314	62,478	8,916	95,337,708	− .011
41	68,921	.024	110,687,126	65,682	8,230	110,761,038	+ .009
43	79,507	.023	127,688,242	68,886	7,887	127,765,015	− .008
45	91,125	.022	146,346,750	72,090	7,544	146,426,384	+ .007
47	103,823	.021	166,739,738	75,294	7,201	166,822,233	− .006
49	117,649	.020	188,944,294	78,498	6,558	189,029,650	+ .005
51	132,651	.020	213,027,506	81,702	6,858	213,126,066	− .005
53	148,877	.019	239,096,462	84,906	6,515	239,187,883	+ .004
55	166,375	.018	267,198,250	88,110	6,172	267,292,532	− .004
57	185,193	.018	297,419,958	91,314	6,172	297,517,444	+ .003
59	205,379	.017	329,838,674	94,518	5,830	329,939,022	− .003
61	226,981	.016	364,531,486	97,722	5,487	364,634,695	+ .003
63	250,047	.016	401,575,482	100,926	5,487	401,681,895	− .003
65	274,625	.015	441,047,750	104,130	5,144	441,157,024	+ .002
67	300,763	.015	482,880,838	107,334	5,144	482,993,316	− .002
69	328,509	.014	527,585,454	110,538	4,801	527,700,793	+ .002
71	357,911	.014	574,805,066	113,742	4,801	574,923,609	− .002
73	389,017	.014	624,761,302	116,946	4,801	624,883,049	+ .002
75	421,875	.013	677,531,250	120,150	4,458	677,655,858	− .001
							−0.03

TABLE 4. SUMMATION OF TRANSVERSE HARMONIC CONTRIBUTIONS TO THE AXIAL STRAIN

ϕ	$1 \cos\phi$	$3.56 \cos 2\phi$	$1.92 \cos 3\phi$	$0.13 \cos 4\phi$	$-0.03 \cos 5\phi$	$\frac{0.0613 \times 10^6}{q} \frac{\partial u}{\partial x}$
0	1.000	3.56	1.92	0.13	−0.03	6.58
15	0.966	3.08	1.36	.065	− .007	5.46
30	.866	1.78	0	−0.065	.026	2.61
45	.707	0	−1.36	−0.13	.021	−0.76
55	.574	−1.22	−1.86	− .10	− .003	−2.61
65	.423	−2.29	−1.86	− .023	− .025	−3.775
75	.259	−3.08	−1.36	.065	− .029	−4.145
80	.174	−3.35	−0.96	.10	− .023	−4.06
90	0	−3.56	0	.13	0	−3.43
105	−0.259	−3.08	1.36	.065	0.027	−1.89
125	− .574	a1.22	1.86	.10	.003	0.17
135	− .707	0	1.36	− .013	− .021	.62
150	− .866	1.78	0	− .065	− .026	.82
180	−1.000	3.56	−1.92	0.13	0.03	0.80

CHANGE IN TRANSVERSE CURVATURE AT MID-SPAN CROSS-SECTION FOR THE UNIFORM RADIAL LINE LOAD EXTENDING ALONG THE TOP GENERATRIX

$$\frac{1.14 \times 10^2}{q} \chi_\varphi = \sum_{m,n}^{\infty} \frac{(1-n^2)\cos n\varphi \sin\frac{m\pi}{2}}{m^5\left[\frac{10^6}{n^4} + 595.33\left(\frac{1-n^2}{m^2}\right)^2 + 46.05\left(\frac{n}{m}\right)^2\right]}$$

TABLE 5. TRANSVERSE HARMONIC CONTRIBUTIONS TO χ_ϕ

n	$\cos n\phi$	$n^2 - 1$	Σ (See page 19)	$\frac{1.14 \times 10^2}{q} \chi_\phi$
1	$\cos\phi$	0	0.966	0
2	$\cos 2\phi$	−3	14.65	$-43.95 \cos 2\phi$
3	$\cos 3\phi$	−8	19.39	$-155.1 \cos 3\phi$
4	$\cos 4\phi$	−15	6.56	$-98.3 \cos 4\phi$
5	$\cos 5\phi$	−24	2.33	$-55.7 \cos 5\phi$
6	$\cos 6\phi$	−35	1.03	$-36.1 \cos 6\phi$
7	$\cos 7\phi$	−48	0.58	$-27.8 \cos 7\phi$
8	$\cos 8\phi$	−63	0.33	$-21.0 \cos 8\phi$
9	$\cos 9\phi$	−80	0.17	$-13.6 \cos 9\phi$
10	$\cos 10\phi$	−99	0.09	$9.0 \cos 10\phi$
11	$\cos 11\phi$	−120	0.05	$6.0 \cos 11\phi$
12	$\cos 12\phi$	−143	0.03	$4.3 \cos 12\phi$
13	$\cos 13\phi$	−168	0.02	$3.4 \cos 13\phi$
14	$\cos 14\phi$	−195	0.01	$2.0 \cos 14\phi$

TABLE 6. SUMMATION OF THE TRANSVERSE HARMONIC CONTRIBUTIONS TO THE CHANGE IN TRANSVERSE CURVATURE, χ_ϕ

ϕ	$43.95 \cos 2\phi$	$155.1 \cos 3\phi$	$98.3 \cos 4\phi$	$55.7 \cos 5\phi$	$36.1 \cos 6\phi$	$27.8 \cos 7\phi$	$21.04 \cos 8\phi$	$13.6 \cos 9\phi$	$9 \cos 10\phi$	$6 \cos 11\phi$	$4.3 \cos 12\phi$	$3.4 \cos 13\phi$	$2 \cos 14\phi$	$\frac{1.14 \times 10^2}{q} \chi_\phi$
0	43.95	155.1	98.3	55.7	36.1	27.8	21.042	13.6	9.0	6.0	4.3	3.4	2.0	476.3
10	41.0	134.3	75.4	35.8	18.0	9.5	3.6	0	−1.5	−2.1	−2.2	−2.2	−1.5	308.1
20	33.4	77.6	17.1	− 9.7	−18.0	−21.2	−19.8	−13.6	−8.5	−4.6	−2.2	−0.6	0.4	29.6
30	21.8	0	−49.2	−48.2	−36.1	−24.1	−10.6	0	4.6	5.2	4.3	2.9	1.0	−128.4
40	7.6	− 77.6	−92.4	−52.4	−18.0	4.8	16.1	13.6	6.9	1.0	−2.2	−3.2	−1.9	−197.7
50	−7.6	−134.3	−92.4	−19.1	+18.0	27.3	16.1	0	−6.9	−5.9	−2.2	1.2	−1.9	−207.7
60	−21.8	−155.1	−49.2	27.9	+36.1	13.9	−10.6	−13.6	−4.6	3.0	4.3	1.7	−1.0	−172.0
70	−33.4	−134.3	17.1	54.9	+18.0	−18.0	−19.8	0	8.5	3.9	−2.2	−3.3	−0.4	−109.0
80	−41.0	− 77.6	75.4	42.7	−18.0	−26.1	3.6	13.6	1.5	−5.6	−2.2	2.6	1.5	− 29.6
90	−43.95	0	98.3	0	−36.1	0	21.042	−9.0	0	4.3	0	−2.0	−2.0	32.5
100	−41.0	77.6	75.4	−42.7	−18.0	26.1	3.6	−13.6	1.5	5.6	−2.2	−2.6	1.5	71.2

APPENDIX B

References:

1. A Treatise on the Mathematical Theory of Elasticity, by A. E. H. Love, Fourth Edition, Dover Publication, 1944, ch 24.

2. Theory of Plates and Shells, by S. Timoshenko, McGraw-Hill Book Co., 1940, ch 11.

3. "Technical Report No. 1 on the Equations of Motion of Cylindrical Shells", by P. M. Naghdi and J. G. Berry, Engineering Research Institute, University of Michigan, U. S. Navy Proj. No. 2041-3, April 1953.

4. "Line Load Action on Thin Cylindrical Sheels", by H. Schorer, ASCE 1936, vol 101, p 767.

5. Strength of Materials, Part II, by S. Timoshenko, D. Van Nostrand Company, Inc., 1941, p 47.

6. "Thin Cylindrical Shells Subjected to Concentrated Loads", by S. W. Yuan, Quarterly of Applied Mathematics, Vol 4, No. 1, (1946).

7. "The New Approach to Shell Theory: Circular Cylinders", by E. H. Kennard, Journal of Applied Mechanics, vol 20, No. 1 (1953).